NASA CR-144680

REAL-TIME ORBIT ESTIMATION FOR ATS-6 FROM REDUNDANT ATTITUDE SENSORS

Thomas S. Englar, Jr.

Business and Technological Systems, Inc.
Aerospace Building, Suite 605
10210 Greenbelt Road
Seabrook, Maryland 20801

April 1975

Final Report BTS-TR-75-20

Prepared for

GODDARD SPACE FLIGHT CENTER
Greenbelt, Maryland 20771

1. Report No.	2. Government Accession No.	3. Recipient's Catalog No.
BTS-TR-75-20		

4. Title and Subtitle	5. Report Date
REAL-TIME ORBIT ESTIMATION FOR ATS-6 FROM REDUNDANT ATTITUDE SENSORS	April 1975
	6. Performing Organization Code
7. Author(s) Thomas S. Englar, Jr.	8. Performing Organization Report No. BTS-TR-75-20
9. Performing Organization Name and Address Business and Technological Systems, Inc. 10210 Greenbelt Road, Suite 605 Seabrook, Maryland 20801	10. Work Unit No.
	11. Contract or Grant No. NAS 5-20844
	13. Type of Report and Period Covered Final Report
12. Sponsoring Agency Name and Address Goddard Space Flight Center Greenbelt, Maryland 20771 Mr. J. Maury	14. Sponsoring Agency Code

15. Supplementary Notes

16. Abstract

Business and Technological Systems, Inc. has installed a program in the ATSOCC on-line computer which operates with attitude sensor data to produce a smoothed real-time orbit estimate. This estimate is obtained from a Kalman filter which enables the estimate to be maintained in the absence of T/M data. This report describes the results of analytical and numerical investigations into the sensitivity of Control Center output to the position errors resulting from the real-time estimation.

The results of the numerical investigation, which used several segments of ATS-6 data gathered during the Sensor Data Acquisition run on August 19, 1974, show that the implemented system can achieve absolute position determination with an error of about 100 km, implying pointing errors of less than 0.2° in latitude and longitude. This compares very favorably with ATS-6 specifications of approximately 0.5° in latitude-longitude.

17. Key Words (Selected by Author(s))	18. Distribution Statement
Real-Time Orbit Determination, Real-Time Filtering, S/C Pointing Accuracy	

19. Security Classif. (of this report)	20. Security Classif. (of this page)	21. No. of Pages	22. Price*
Unclassified	Unclassified	63	

*For sale by the Clearinghouse for Federal Scientific and Technical Information, Springfield, Virginia 22151.

TABLE OF CONTENTS

		Page
1.0	INTRODUCTION AND SUMMARY	1-1
2.0	SENSITIVITY ANALYSIS	2-1
3.0	NUMERICAL RESULTS	3-1
4.0	CONCLUSIONS AND RECOMMENDATIONS	4-1

1.0 INTRODUCTION AND SUMMARY

Business and Technological Systems, Inc. has installed a program in the ATSOCC on-line computer which operates with attitude sensor data to produce a smoothed real-time orbit estimate. This estimate is obtained from a Kalman filter which enables the estimate to be maintained in the absence of T/M data. This report describes the results of analytical and numerical investigations into the sensitivity of Control Center output to the position errors resulting from the real-time estimation.

The results of the numerical investigation, which used several segments of ATS-6 data gathered during the Sensor Data Acquisition run on August 19, 1974, show that the implemented system can achieve absolute position determination with an error of about 100 km, implying pointing errors of less than 0.2° in latitude and longitude. This compares very favorably with ATS-6 specifications of approximately 0.5° in latitude-longitude.

2.0 SENSITIVITY ANALYSIS

While S/C position is a very essential piece of information in computing S/C attitude or pointing vector, these output variables are relatively insensitive to changes in S/C position. Primarily this occurs because of the 6.62 ratio between the radii of the orbit and the Earth. In the current study, it was necessary to consider several distinct sensitivities:

a) Sensitivity of subpoint to S/C position.

b) Sensitivity of S/C attitude to S/C position.

c) Sensitivity of pierce point to S/C position.

d) Sensitivity of "sensed" S/C position to errors in sensor data.

e) Sensitivity of S/C pointing vector to S/C attitude.

One of the purposes of the current task was to create a program for the PDP-11 which would mechanize the triangulation for position-sensing and run a Kalman filter to smooth these "sensed" values. A second purpose was to perform a study evaluating the effect on S/C attitude and pointing vector of the position errors incurred by this real-time orbit determination. Clearly all of the sensitivities mentioned above are relevant to these purposes.

For that reason it appears valuable to collect what analytic information is available on these sensitivities.

For these calculations we take the radius of the Earth to be

$$R = 6378 \text{ km}$$

and the nominal ATS-6 orbit radius to be

$$r = 42164 \text{ km.}$$

2.1 Sensitivity of Subpoint to S/C Position

Except for Earth flattening effects, the sensitivity of subpoint to position is given by the ratio of radii. That is, sensitivity to changes along the radius vector are zero; sensitivity of subpoint position to changes normal to the radius vector is $1/6.62 = 0.151$.

$$\frac{\partial x_{sp}}{\partial x_{sc}} = 0.151. \tag{2.1}$$

The relations between position and central angle are

$$\frac{\partial x_{sp}}{\partial \alpha} = 111 \text{ km/deg} \tag{2.2}$$

$$\frac{\partial x_{sc}}{\partial \alpha} = 736 \text{ km/deg} \quad . \tag{2.3}$$

2.2 Sensitivity of S/C Attitude and Pierce Point to S/C Position

The difficulty with this question is that it is not well posed. There are at least three modes in which the S/C position could be changed. The S/C attitude could remain constant in inertial space; it could remain constant in the (changed) ARS*; or the sensor output could remain constant. All of these are analyzed here; however, it appears that, in general, constant inertial attitude is irrelevant; constant ARS attitude would be the applicable analysis if the computer (or S/C) were operating in an open-loop mode with no sensor data; constant sensor output is the correct model for normal operation.

(1) Constant Inertial Attitude

The S/C is at (x,0,0) and pointing at the Earth center. An increment in y is given but the S/C attitude is unchanged. The pointing vector now intersects the Earth at a new point displaced by the angle θ, where

$$\sin \theta = \frac{y}{R} \quad .$$

We thus have that

$$\frac{d\theta}{dy} = \frac{1}{R \cos \theta} \quad .$$

Thus, the sensitivity of pierce point latitude or longitude at the sensitivity of S/C attitude with respect to the ARS to cross track or downtrack position errors

*ARS denotes the Attitude Reference System, which for ONATT is an orthogonal, S/C-centered coordinate system with $\hat{z}$ pointed to Earth center, $\hat{y}$ pointed south, and $\hat{x}$ east.

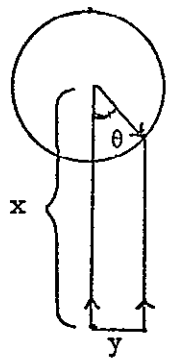

$$R \sin \theta = y$$

Fig. 1

Case (1) Geometry

is approximately

$$0.16E\text{-}3 \text{ rad/km}$$

or

$$0.009^\circ \text{ (lat/long)/km} \quad . \tag{2.4}$$

(2) Constant Attitude WRT ARS

The S/C is at (x,0,0) and pointing at the Earth center. An increment in y is given and the S/C rotates so as to remain pointing down the local vertical. The pointing vector now intersects the Earth at a new point displaced by the angle θ, where

$$\tan \theta = \frac{y}{x} \quad .$$

We thus have that

$$\frac{d}{dy} = \frac{\cos^2\theta}{x} \quad .$$

Thus, the sensitivity of pierce point lat/long with respect to cross track or downtrack position errors is approximately

$$\frac{d\theta}{dy} = 2.3 \text{ E-5 rad/km}$$

or (2.5)

$$1.36 \text{ E-3}^\circ \text{ (lat/long)/km} \quad .$$

(3) Sensor Output Constant

When this mode is considered, some of the difficulties of the problem become very clear. Suppose that Polaris lay on the polar axis and the ESA/PSA combination were used for attitude determination. Then changes in S/C position, together with attitude changes keeping sensor output constant, would produce no change in attitude with respect to the ARS. All changes in the pointing vector, then, would occur

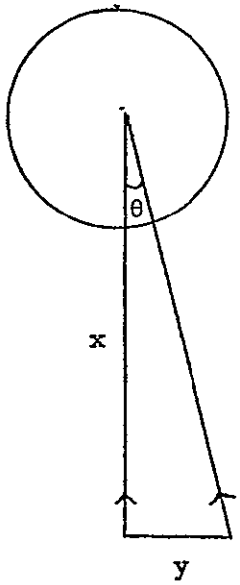

$$\tan \theta = \frac{y}{x}$$

Fig. 2

Case (2) Geometry

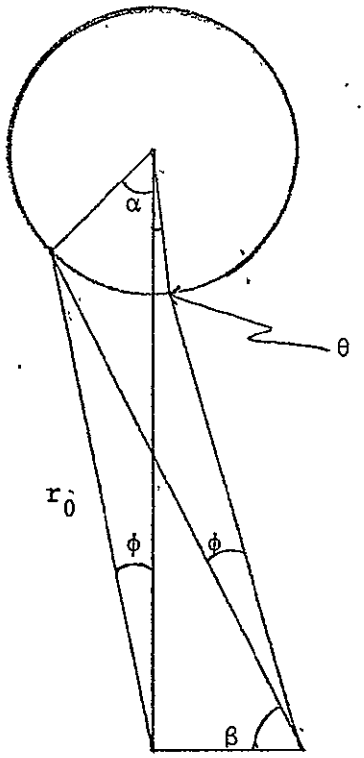

Fig. 3

Case (3) Geometry

from changes in the subpoint and (2) and (3) are identical for such an ESA/PSA.

In actual practice, Polaris lies off the polar axis and therefore a change in S/C position can change the attitude in yaw. Through coupling, this can then change roll and pitch attitude. These are second order effects, however, and when ESA/PSA is used for attitude control, it seems proper to say that the sensitivity of attitude to position change is zero and that sensitivity of pierce point to position is as given in 2.1.

Consider the S/C at (x,0,0) pointing at EC and an illuminator at longitude α. An increment in y is given and the S/C rotates so as to keep invariant the angle ϕ to the illuminator. The pointing vector now intersects the Earth at a new point displaced by the angle θ.

The global relationship between y and θ is exceedingly complicated and since we are only interested in local sensitivity, let us deal with incremental values. Using the law of sines and an intermediate angle β, we find that

$$\frac{\sin \beta}{r_0} = \frac{\cos(\phi+\beta)}{y} \quad .$$

Differentiating this and evaluating at $y = 0$, $\beta = \phi$, we obtain

$$\frac{d\beta}{dy} = -\frac{\cos \phi}{r_0} \quad .$$

The differential change in central angle, γ, is of course,

$$d\gamma = \frac{1}{x}\, dy \quad .$$

The angle, n, between the LOS to EC and to the illuminator satisfies

$$\beta + n = 90 - \gamma \quad ,$$

and to keep the sensor output constant, we require that

$$n + p = \phi \quad ,$$

where p is the pitch angle.

It follows that

$$\beta + \phi - p = 90 - \gamma$$

or

$$dp = d\beta + d\gamma \quad .$$

Using the formulae now available,

$$dp = \left[-\frac{\cos \phi}{r_0} + \frac{1}{x} \right] dy \quad .$$

Taking nominal values (for Rosman) of

$$\phi = 3.771°$$

$$r_0 = 36329 \text{ km}$$

we obtain

$$\frac{dp}{dy} = -3.75E\text{-}6 \text{ rad/km} = -2.15E\text{-}4°/\text{km} \quad . \tag{2.6}$$

This gives the sensitivity of attitude to position when using an interferometer at Rosman to perform attitude control.

Defining the new pierce point by

$$(R \cos \theta, R \sin \theta),$$

we find that

$$R \cos \theta = x - \ell \cos (90-\beta-\phi)$$
$$R \sin \theta = y - \ell \sin (90-\beta-\phi)$$

where ℓ is the unknown distance from S/C to pierce point. These can be solved to obtain

$$\tan\ (90-\beta-\phi) = \frac{y-R\ \sin\ \theta}{x-R\ \cos\ \theta}\ .$$

Differentiating this gives

$$\frac{-d\beta}{\cos^2(90-\beta-\phi)} = \frac{dy-R\cos\theta d\theta}{x-R\cos\theta} - \frac{y-R\sin\theta}{(x-R\cos\theta)^2}\ R\ \sin\ \theta d\theta\ .$$

The previously derived expression for $d\beta$ can be used and the formula evaluated at $y = 0$, $\theta = 0$, $\beta = 90 - \phi$, to obtain

$$\frac{d\theta}{dy} = \frac{1}{R} - \frac{(x-R)\cos\phi}{Rr_0}\ .$$

Using the numerical vlues previously derived for Rosman, we have

$$\begin{aligned}\frac{d\theta}{dy} &= 1.568E-4 - 1.541E-4 \\ &= 2.7E-6\ \text{rad/km} \\ &= 1.54E-4°/\text{km}\end{aligned} \qquad (2.7)$$

Thus we see that when the interferometer is used for attitude control, there will be a change in attitude caused by position, but the sensitivity of pierce point is very small since this almost compensates the change in subpoint.

These examples serve to illustrate the problems involved in giving a concise answer to the question of pierce-point or attitude sensitivity to position. Because DOC usually controls with ESA/PSA, this combination was used to generate the numerical studies described in Section 3.

2.3 Sensitivity of "Sensed" S/C Position to Sensor Errors

In theory, the sensitivity of sensed S/C positions to errors in sensor output can be as much as

$$\frac{dx}{d\ell} = 10000\ \text{km/deg} \qquad (2.8)$$

The sensitivity given here varies of course with S/C attitude, which sensor is in error, etc. However, the number is approximately correct. Some analytic examples will be given below.

Since the quantization of interferometer readings is 0.0014° and that of ESA about 0.005°, the errors on a quantization basis alone range as high as 50 km. There is a serious problem with word length in the OCPS calculation, however, and these accuracies are barely achieved (see Section 3) either because of large variations in sensor readings, or because of truncation in the PDP-11.

Example 1: The following analysis gives a figure of 9600 km/deg. Looking at Figure 4, suppose that the ESA is giving correct readings but the IF is in error. In order to preserve the ESA data and correct the IF data, the S/C estimate must move on the line pointing S/C and Earth center. To determine the sensitivity, we must compute $\frac{dr}{d\alpha}$. From the law of sines

$$R \sin \gamma = r \sin \alpha$$

and therefore

$$R \sin (\alpha+\beta) = r \sin \alpha \quad .$$

From this we have that

$$\frac{dr}{d\alpha} = \frac{r\cos\alpha - R\cos(\alpha+\beta)}{\sin\alpha} \quad .$$

Letting $\beta = 22°$ as before, we have that $\alpha = 3.771°$ and

$$\frac{dr}{d\alpha} \approx -9640 \text{ km/deg} \quad . \tag{2.9}$$

Example 2: Another verification of the sensitivity arises from the following special case analysis:

The approximate coordinates of Rosman, Mojave and Earth center are

2.12E6ft	-1.70E7	1.20E7	lat 35°12'	long 277°7'
7.73E6ft	-1.52E7	1.20E7	lat 35°19'	long 243°7'
0,	0,	0.		

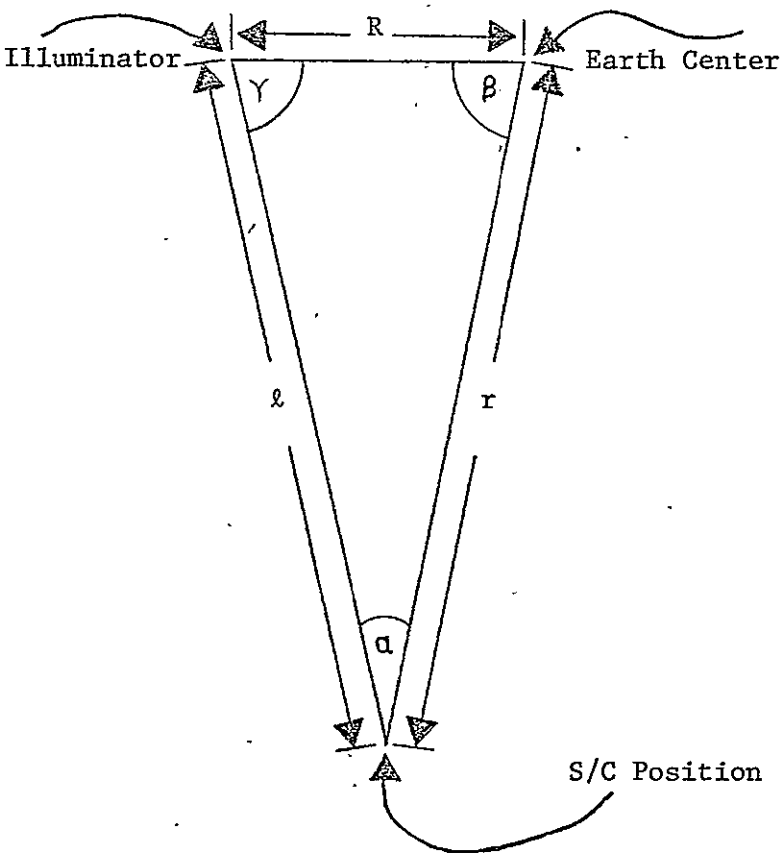

Fig. 4

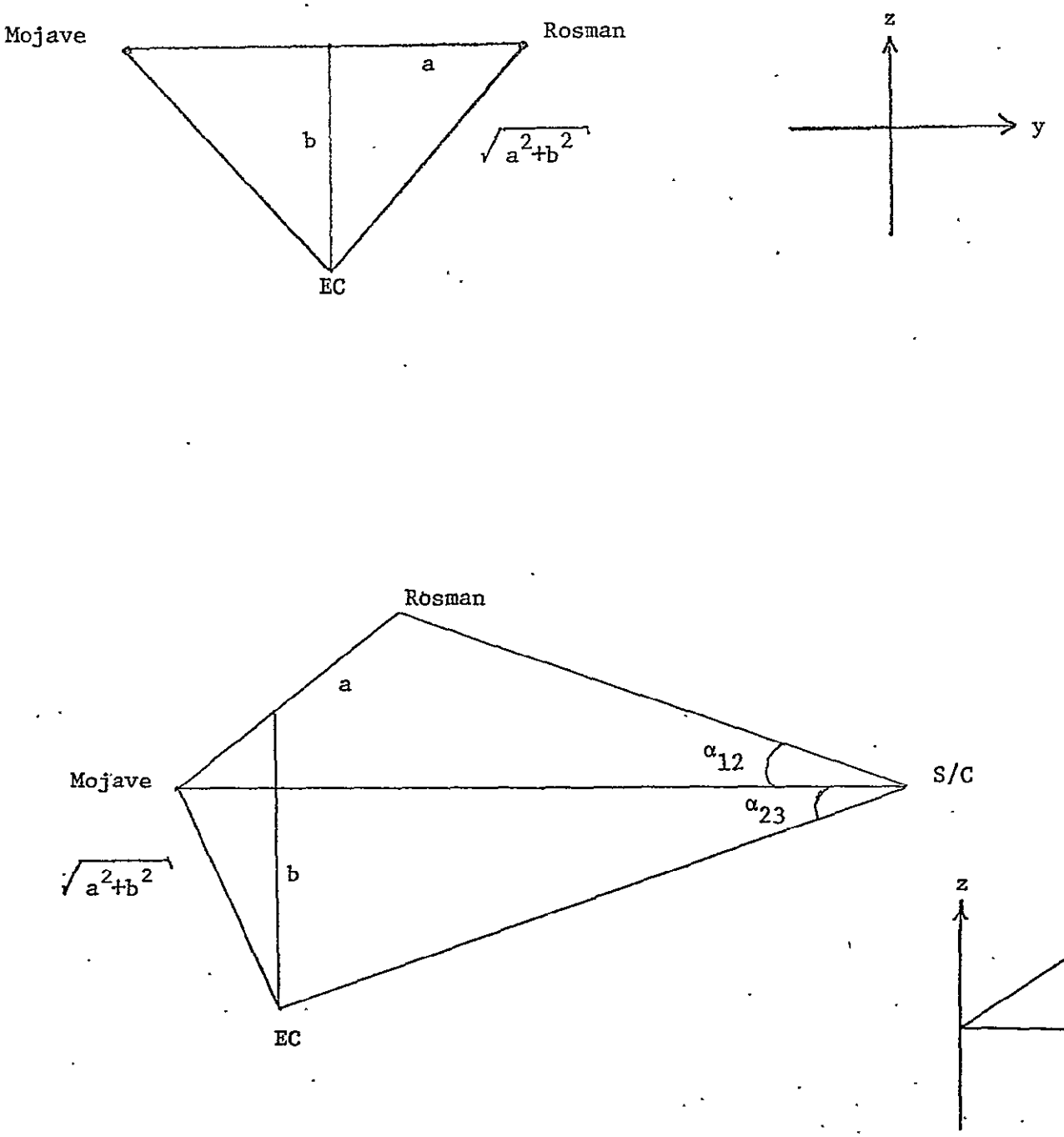

Fig. 5

OCPS Special Case Geometry

Let us take a hypothetical S/C in equatorial synchronous orbit over longitude 260°7' (-99°53'). Then by a rotation of coordinates first about z, then about y, and rounding numbers slightly, this configuration can be represented as

Rosman	(0, .5E7, 2E7) = (0,a,b)	
		$a^2 + b^2 = 4.25E14$
Mojave	(0, -.5E7, 2E7) = (0,-a,b)	
Earth Center	(0, 0, 0)	
S/C	(x, 0, z)	

$x = 1.13E8$

$$x^2 + z^2 \equiv r_3^2 = 1.901E16$$

$z = .79E8$

$$x^2 + (z-b)^2 = 1.625E16$$

$$r_1^2 = 1.6275E16$$

Now let us suppose that the LOS vectors to Rosman and Mojave are measured correctly so that cos α_{12} is also correct;

$$\alpha_{12} = 2 \tan^{-1} \left(\frac{a}{\sqrt{x^2+(z-b)^2}}\right)$$

(nominal value, $\alpha_{12} \simeq 4.492°$)

and suppose that there is an error in the z-component of LOS to the Earth center, but that the y-component is correct (=0). Then the S/C will have to change its x and z coordinates (subject to constant $x^2 + (z-b)^2$) so as to obtain the observed values

$$\alpha_{13} = \alpha_{23},$$

(nominal value, $\alpha_{23} \simeq 7.720$) while holding α_{12} constant.

In this very special case we have

$$x^2 + (z-b)^2 \text{ constant}$$

or

$$xdx + (z-b)dz = 0 \quad . \tag{2.10}$$

Also

$$a^2 + b^2 = r_3^2 + r_1^2 - 2r_1r_3\cos\alpha_{23} \quad ,$$

so

$$(r_3 - r_1\cos\alpha_{23})dr_3 = r_1r_3d\cos\alpha_{23} \quad .$$

Since

$$r_3^2 = x^2 + z^2$$

we have

$$r_3dr_3 = xdx + zdz \quad .$$

Using (2.10) we obtain

$$r_3dr_3 = bdz$$

so that

$$\frac{dz}{d\cos\alpha_{23}} = \frac{r_1r_3^2}{b(r_3 - r_1\cos\alpha_{23})}$$

Evaluating this at the unperturbed position, we have

$$\frac{dz}{d\cos\alpha_{23}} = 1.06E10\text{ft.} \tag{2.11}$$

We now need to determine the sensitivity of $\cos\alpha_{23}$ to errors in the z component of ESA LOS. Up to this point, the analysis has been attitude-independent. Now the attitude must enter. We know that

$$\cos\alpha_{23} = \ell_1 m_1 + \ell_2 m_2 + \ell_3 m_3$$

and

$$m_1 = \sqrt{1-m_2^2-m_3^2} \quad .$$

Since approximately, $\ell_1 = m_1 = 1$, we can say that

$$\frac{\partial \cos\alpha_{23}}{\partial m_3} = \ell_3 - m_3$$

This quantity is almost independent of attitude, and is approximately the sine of the difference in S/C angle between Mojave and Earth center, i.e.

$$\frac{\partial \cos\alpha_{23}}{\partial m_3} \approx \sin\alpha_{23} \approx 0.13$$

We conclude that

$$0 \leq \left|\frac{z}{m_3}\right| \leq 7500 \text{ km/deg} \quad . \tag{2.13}$$

2.4 Sensitivity of S/C Pointing to Attitude

For a fixed subpoint, the pierce point changes with S/C attitude. At the subpoint the total angle change on the surface is about $\frac{r-R}{R}$ times the space angle change, i.e.

$$\frac{\partial\theta}{\partial\alpha} = 5.6 \quad . \tag{2.14}$$

As the pointing vector moves to the edge of the disc, this sensitivity increases for two reasons. In longitude, the convergence of the meridians increases the sensitivity to pitch in the vicinity of the poles. For either latitude or longitude the sensitivity increases as the pointing vector approaches tangency to the Earth. The derivative of Earth central angle is given by

$$\frac{d\theta}{d\alpha} = \frac{r\cos\alpha}{R\cos(\alpha+\theta)} - 1 \tag{2.15}$$

where α is the S/C angle and θ is the Earth central angle from the subpoint. When $\alpha = \theta = 0$ this gives

$$\frac{d\theta}{d\alpha} = 5.6$$

and when the pierce point is at Rosman ($\alpha = 5.66°$, $\theta = 35°$) then

$$\frac{d\theta}{d\alpha} = 7.67 \qquad (2.16)$$

3.0 NUMERICAL RESULTS

We have studied carefully two data spans made during the ATS-6 sensor calibration maneuvers on August 19, 1974. These covered the periods

08 19 13:01 to 08 19 14:17

during which time the pierce point went from S/C subpoint to Rosman to (0,-47°) with three interferometer calibrations and

08 19 16:06 to 08 19 16:50

during which time the pierce point went from (-15.6,-76.7) to subpoint to Mojave to (44,-138) to (-44,-138) with four calibrations.

In Table 3 appear the pierce point coordinates at the relative times in the two intervals when interferometer calibrations were done. These calibrations are performed after the S/C has achieved equilibrium oscillation in low-jitter mode at the desired pierce point. They provide mark points allowing a rough calculation of attitude versus time.

The coordinate system in which position is expressed is the GRS (Greenwich, Earth-fixed). Variations in $x_3(z)$ are essentially cross-track, $x_2(y)$ radial, and $x_1(x)$ downrange.

Angle	Error	Time	$\tilde{x}$	$\tilde{x}_{Max}$
ϕ	.078°	14:00	$\tilde{x}_3 = 460$	480 at 13:50
θ	.155°	13:28	$\tilde{x}_1 = -846$	-846 at 13:28
ψ	.018°	13:49	$\tilde{x}_1 = -776$	-846 at 13:28
ϕ	.097°	16:06	$\tilde{x}_3 = 560$	634 at 16:32
θ	.166°	16:29	$\tilde{x}_1 = -885$	-880 at 16:33
ψ	.029°	16:30	$\tilde{x}_1 = -885$	-880 at 16:33

Table 1

Maximum Euler Angle Errors

Angle	Error	Time	$\Delta\alpha(x)$	$\Delta\alpha(\theta)$	Total
Lat	-1.17°	14:01	-0.62°	-0.43°	-1.05°
Long	-0.38°	14:01	-1.10°	0.77	-0.33°
Bear	0.04°	13:46			
Lat	-1.06°	16:25	-0.77°	-0.37°	-1.14°
Long	0.46°	16:39	-1.16°	0.90	0.26°
Bear	0.06°	16:40			

Table 2

Maximum Pierce Point Errors

subpt cal at 750 sec.

Rosman cal at 3000 sec.

(0,-47) cal at 4000 sec.

(-15.6,-76.7) cal at 200 sec.

subpt cal at 850 sec.

Mojave cal at 1600 sec.

(44,-138 cal at 2100 sec.

Table 3

Pierce Points in Intervals 1 and 2

3.1 Sensor Errors

Certainly the first question which we wish to answer in this study is how good are the individual pseudo-measurements of position. As we have seen in Section 2.3, the variations in sensed position will certainly be at least 50 km. On the other hand, any inaccuracies in sensor calibration, excessive noise in the sensor, or truncation in the PDP-11 will increase the variation.

The plots of sensed positions versus disc ephemeris show several things: First there are the very large bias offsets. These biases are quite consistent in the two intervals, being about -750 km in x_1 and -450 km in x_3. The offset in x_2 ranges between -40 and -100 km; however, there appears to be an attitude dependent component in all three components of about 100 km and in x_2 this is as large as the bias.

The second striking thing about the plots appears most readily in Figures 3 and 6. This is the 200-300 km change in sensed values of x_3 which take place when the interferometer is in the calibration mode. The calibration mode is a self-calibration capability in which the ends of the interferometer baselines are electronically switched. By comparing the unambiguous counts obtained in cal on with those obtained previously and subsequently in cal off, a partial calibration can be performed on-line without interrupting data flow. If such compensation were performed, the bias in x_3 could be reduced to about -250 km. A small effect of calibration can be seen in x_2 and this is also such as to reduce the bias offset. Unfortunately, no effect of calibration can be seen in x_1, the component with largest error. The effect of calibration compensation on x_3 would be, in itself, sufficient to bring the latitude errors (Table 2) down to about 0.6°.

In looking at the calibration bursts in Figures 3 and 6, two other phenomena are observed. There seems to be considerable attitude dependence appearing in both the offsets and the variance. In Figure 3 for instance, both the offset and the variance appear to be larger at Rosman than at subpoint. In Figure 6, the offset grows as the pierce point goes from the southern hemisphere through the subpoint to Mojave. In Figure 6, the scatter during the calibration at (44,-138) appears significantly larger than at the other points.

The questions which are raised here can be at least partially answered by a thorough analysis of all the data taken during the sensor calibration run. Such an analysis could remove the observed biases and resolve whether the observed changes are attitude dependent or functions of time.

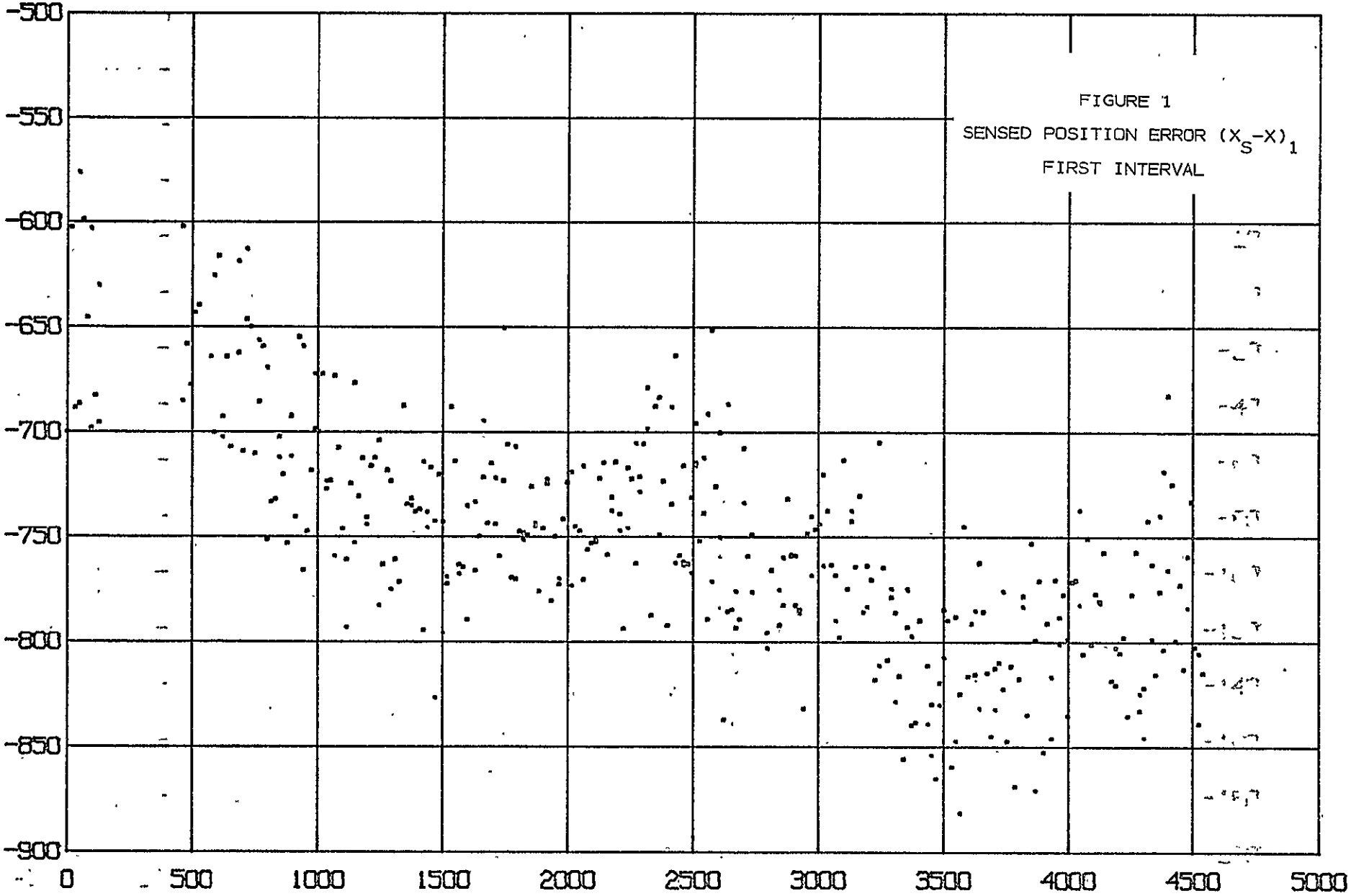

FIGURE 1

SENSED POSITION ERROR $(X_S - X)_1$

FIRST INTERVAL

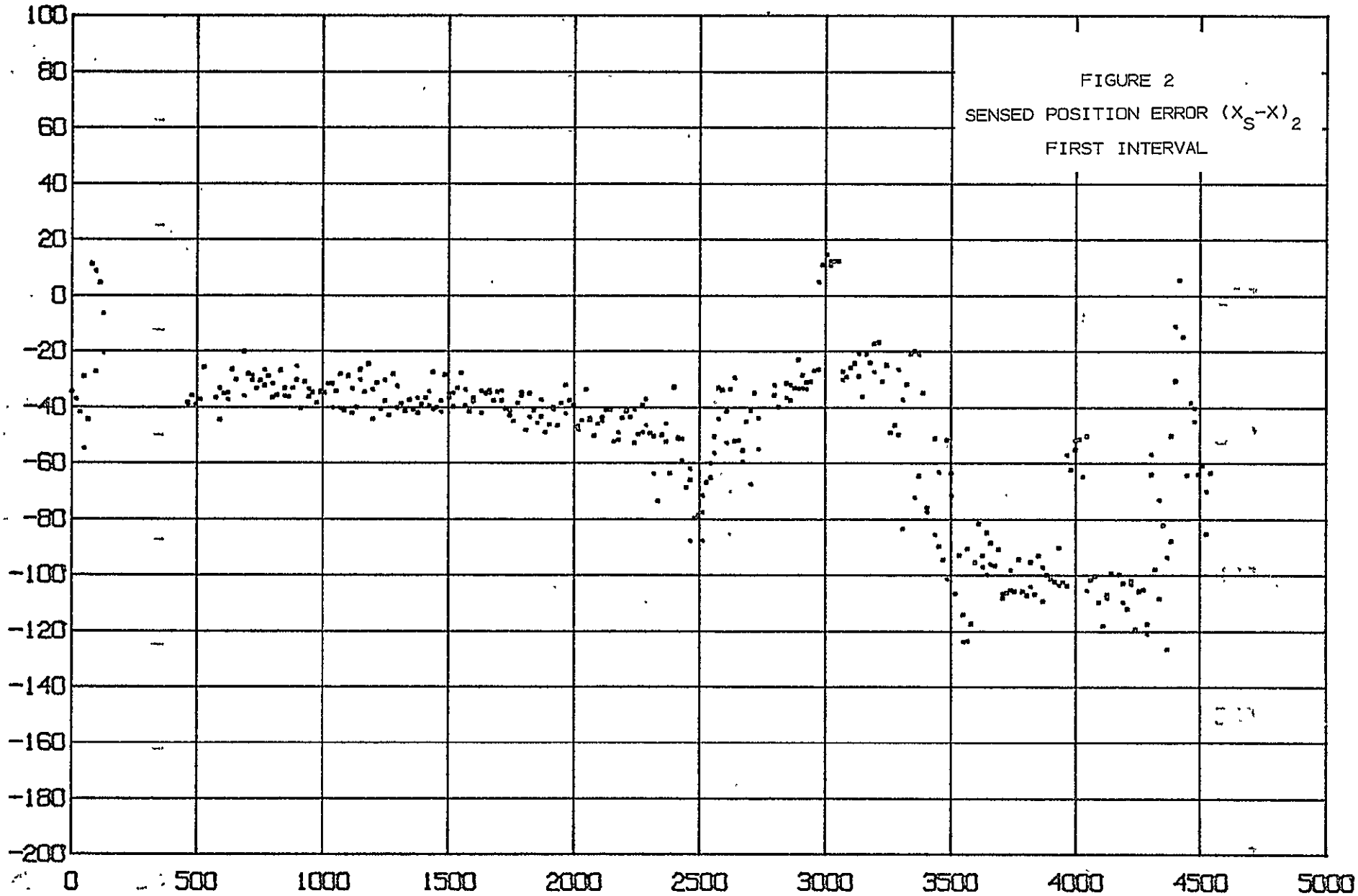

FIGURE 2

SENSED POSITION ERROR $(X_S - X)_2$

FIRST INTERVAL

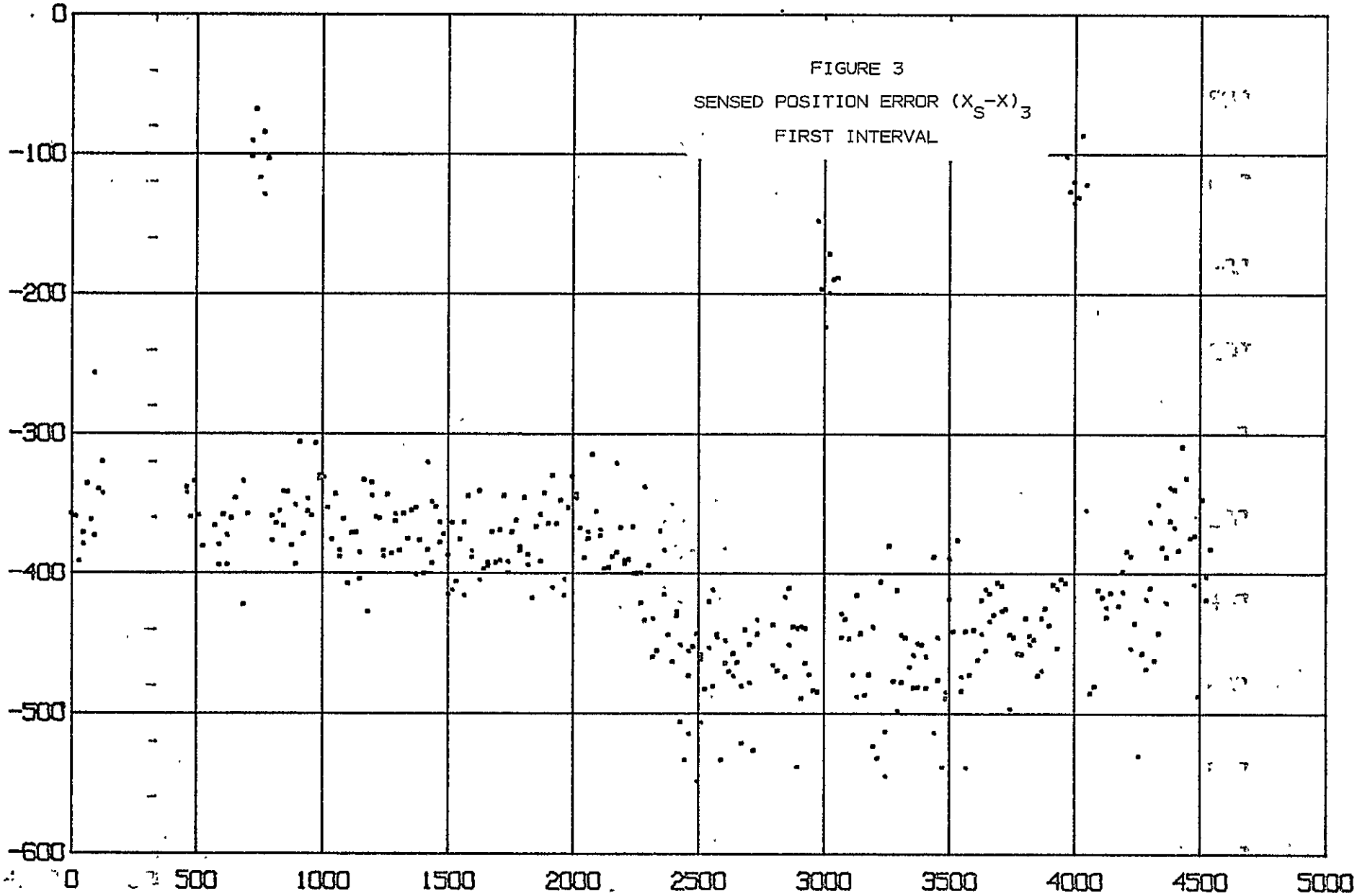
FIGURE 3
SENSED POSITION ERROR $(X_S-X)_3$
FIRST INTERVAL
0
-100
-200
-300
-400
-500
-600
0
500
1000
1500
2000
2500
3000
3500
4000
4500
5000

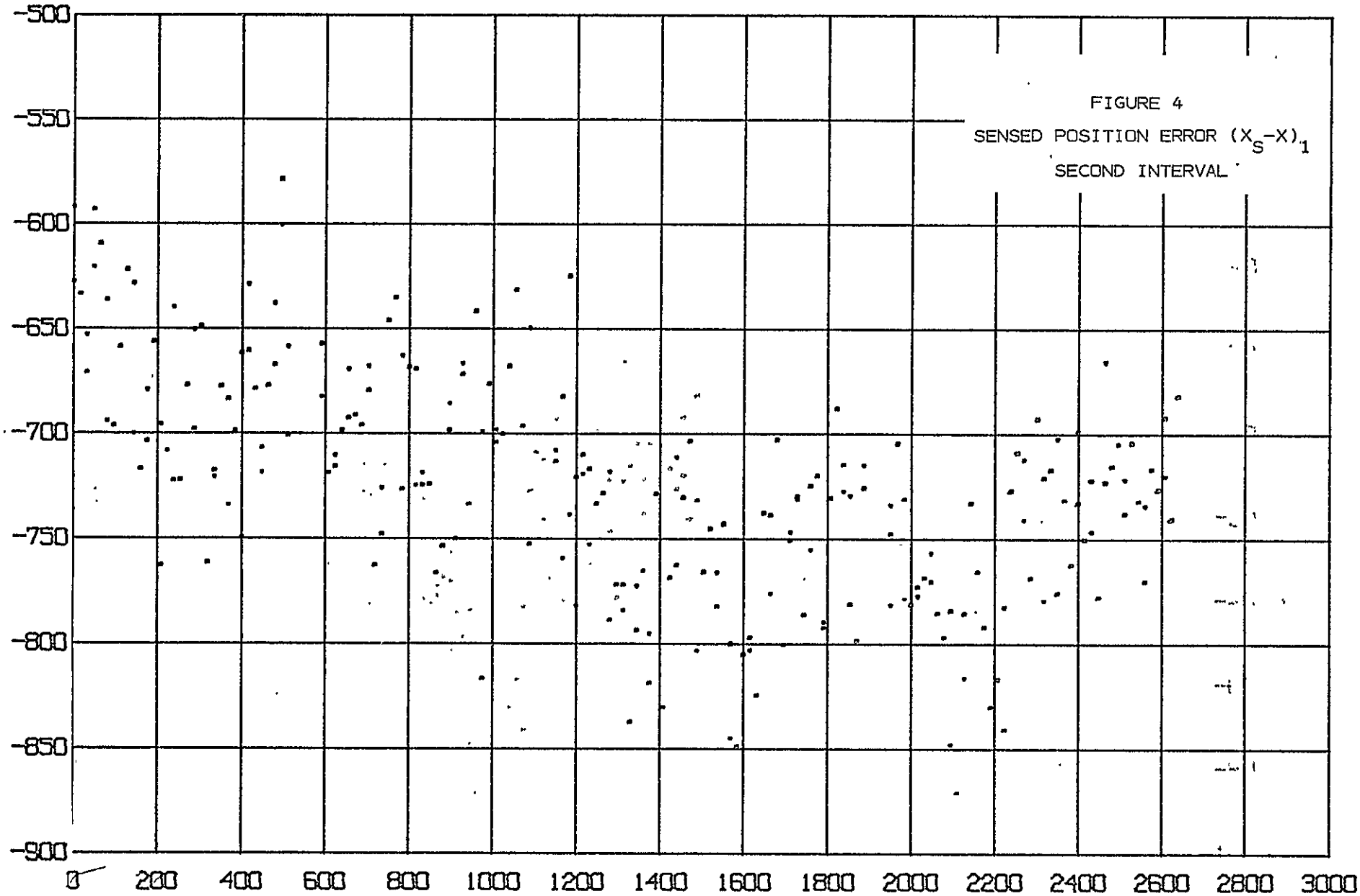

FIGURE 4

SENSED POSITION ERROR $(X_S - X)_1$

SECOND INTERVAL

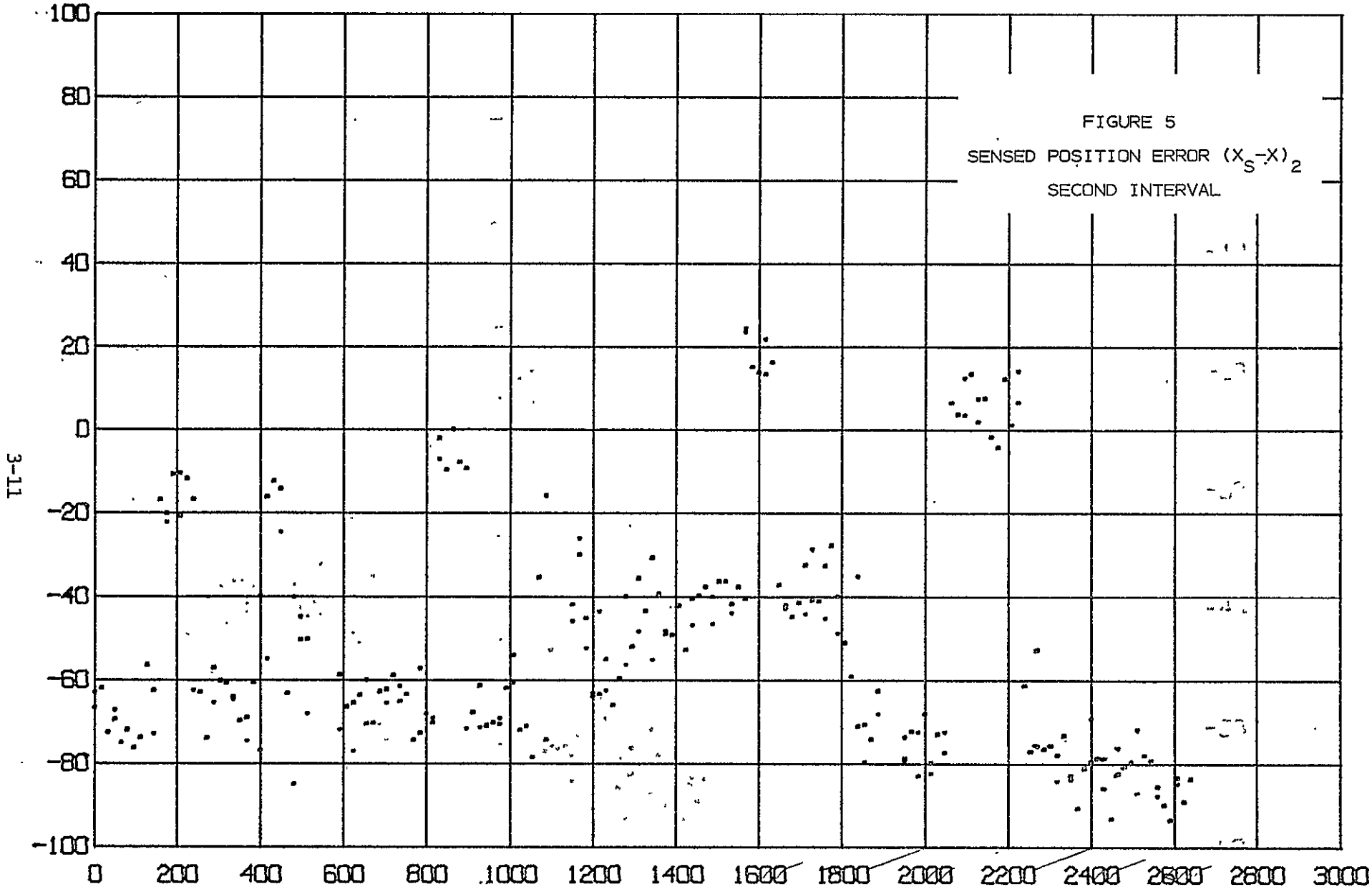

FIGURE 5

SENSED POSITION ERROR $(X_S - X)_2$

SECOND INTERVAL

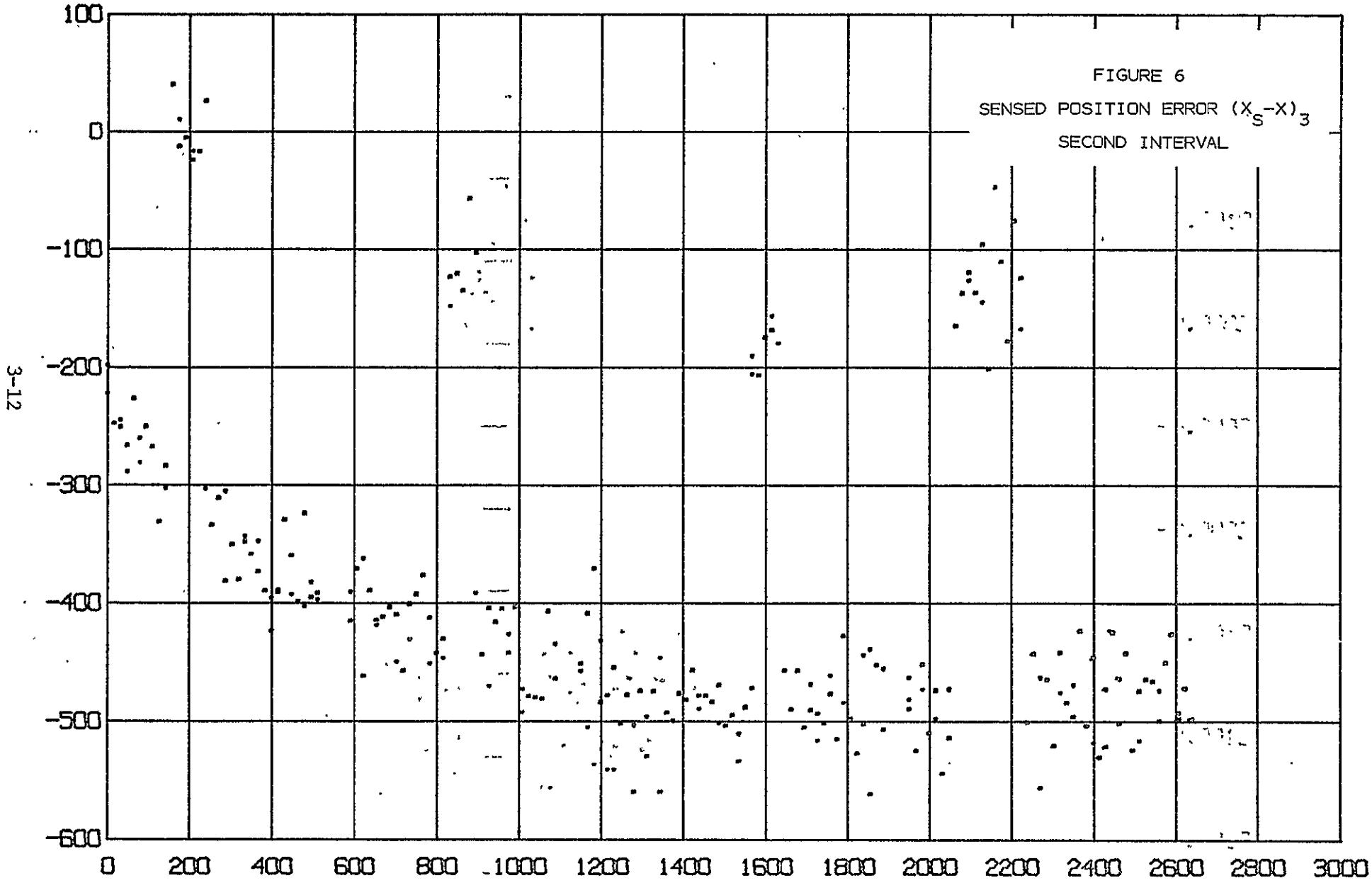

FIGURE 6

SENSED POSITION ERROR $(X_S - X)_3$

SECOND INTERVAL

3.2 Filter Errors

In Figures 7-18 are plotted the filter errors ($x-\hat{x}$) and the filter residuals ($x_s-\hat{x}$) for the two data intervals.

The primary purpose of examining the filter error is to evaluate its dynamic response and observe its variance about itself. Both features appear good in these runs. The time constant for the system is long (*12 min) but the response is quite smooth, with variations of less then 5 km. In an operational system there is no necessity for good step response so the constant gains used here (0.02, 0.0002) are probably close to the desired values.

The x_1 component, Figures 7 and 10, shows classical underdamped step response. Notice that the data gaps disturb the response very little.

The x_3 response, Figures 9 and 12, is also quite satisfactory, showing good tracking of the time-varying values of sensor output. Notice the drastic effects of the calibration.

The x_3 component shows the attitude dependence of the readings very clearly. This component looks very irregular but this is caused by a combination of attitude-dependent effects, calibration errors, and the high resolution of the plot.

Figures 13-18 are graphs of the filter residuals ($x_s-\hat{x}$) which drive the filter. The equilibrium value of this variable should be zero and its variance is a measure of the sensor noise. In all of these plots, it appears that the sensor noise has a standard deviation of about 50 km, with strong time or attitude-dependent fluctuations (Figures 14, 15, 17).

The conclusion to be drawn from these graphs is that the "sensor" noise is approximately as expected and appears to be reasonably well uncorrelated. There is also strong attitude dependency which careful analysis over the disc could probably remove. Neither of these are as serious as the large biases which can certainly be removed by calibration.

Some statistical analysis of the residuals was done, but over the entire data interval which, because of the filter dynamic response gave misleading values of

the variance. When this analysis was performed on the sensor errors, more realistic results were obtained. These are presented in Table 4 and show that the statistics are quite consistent. The variance of x_3 is somewhat larger in interval 2 but this is partially because of the greater effect of calibration. If the calibration outliers had been removed then the standard deviation of 140 would have been reduced to about 110.

Table 4 also shows the time correlation of the signals. The paramter ρ_t is the correlation coefficient of the signal with t and $\rho_t 2$ is the correlation of the signal with the orthogonal component of t^2. Because of the long time interval these remove very little of the high frequency component. Instead they reflect time or attitude dependent trends in the signal.

Interval	Variable	Mean (km)	σ (km)	ρ_t	σ_t (km)	ρ_t^2	σ_t^2 (km)
1	x_s-x_1	-749	54	.71	38	.16	37
1	x_s-x_2	-50	29	.59	23	.16	23
1	x_s-x_3	-390	82	.30	79	.26	76
2	x_s-x_1	-723	54	.54	46	.34	42
2	x_s-x_2	-50	28	.05	28	.32	27
2	x_s-x_3	-384	140	.36	131	.28	125

Table 4

Sensor Noise Characteristics

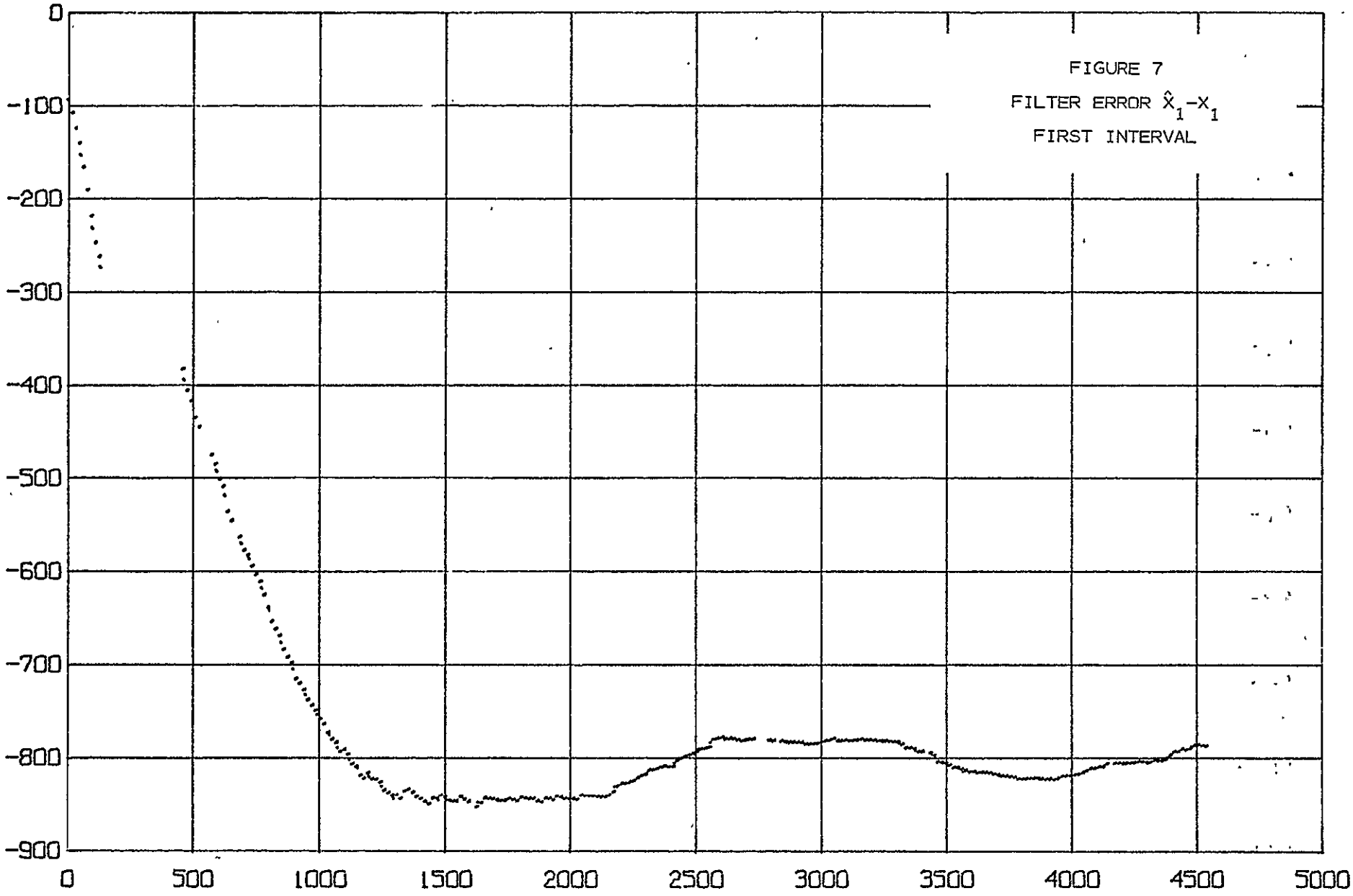
FIGURE 7
FILTER ERROR $\hat{X}_1 - X_1$
FIRST INTERVAL
0
-100
-200
-300
-400
-500
-600
-700
-800
-900
0
500
1000
1500
2000
2500
3000
3500
4000
4500
5000

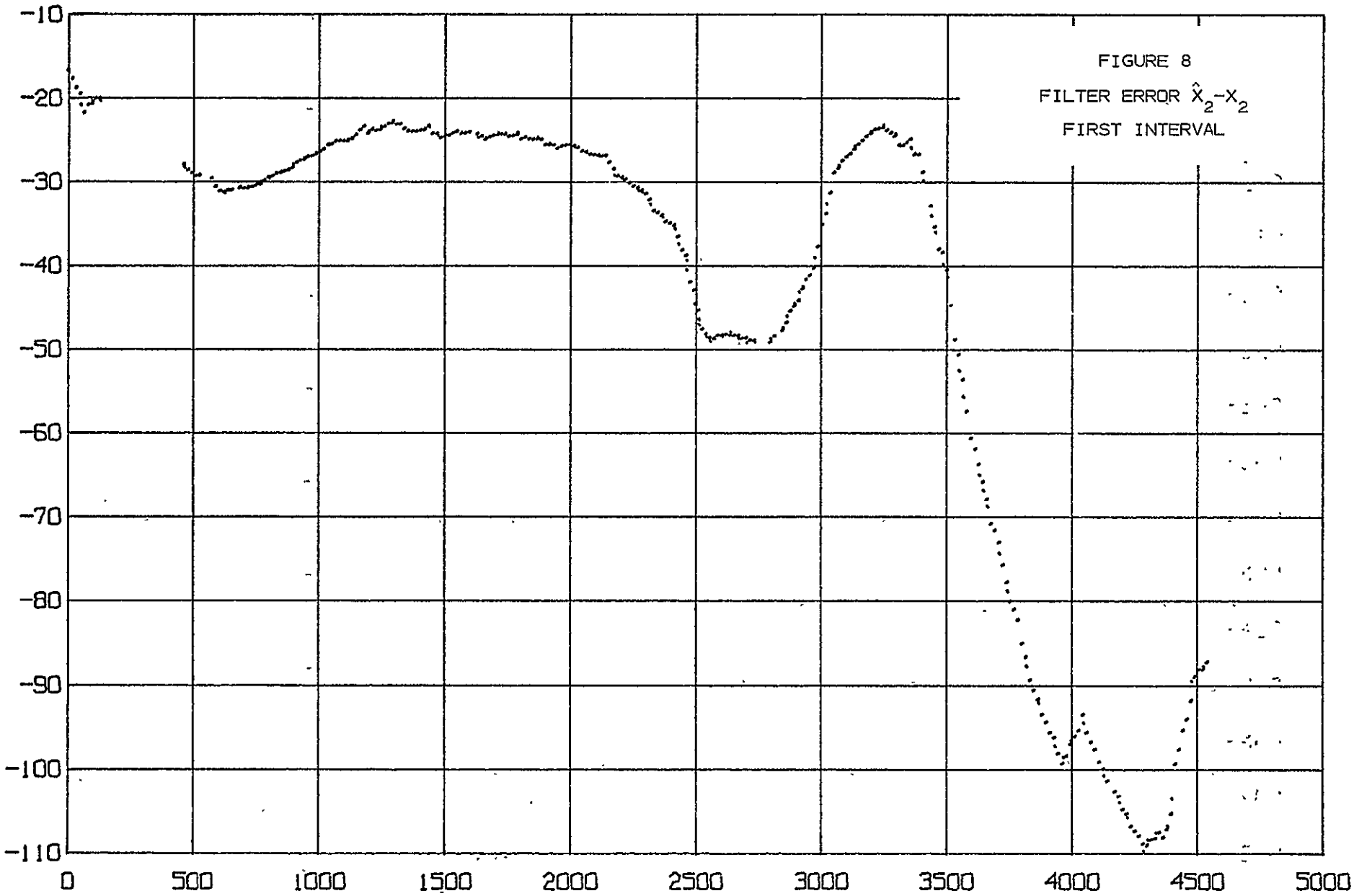

FIGURE 8

FILTER ERROR $\hat{X}_2 - X_2$

FIRST INTERVAL

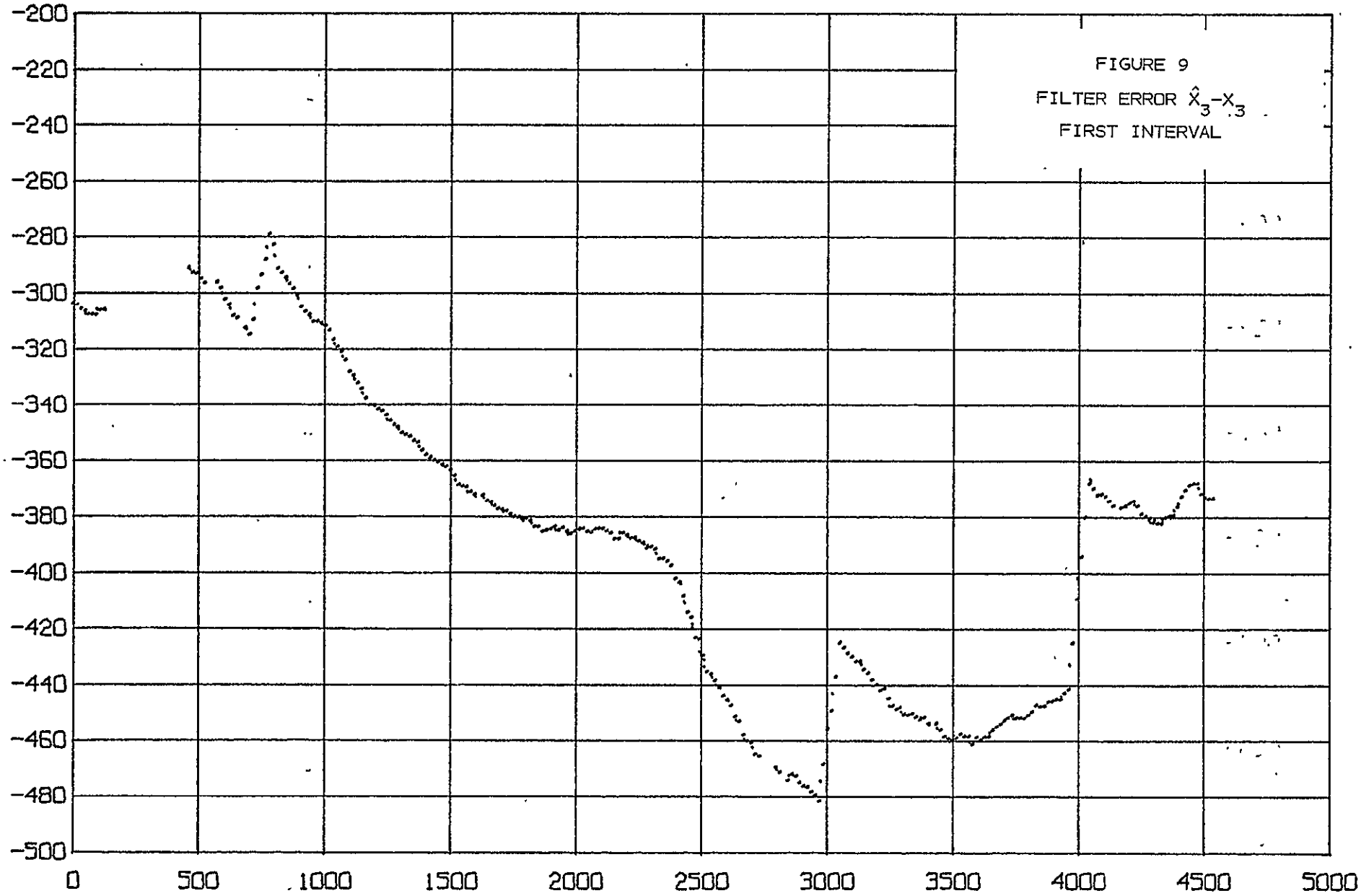
FIGURE 9
FILTER ERROR $\hat{X}_3 - X_3$
FIRST INTERVAL
-200
-220
-240
-260
-280
-300
-320
-340
-360
-380
-400
-420
-440
-460
-480
-500
0
500
1000
1500
2000
2500
3000
3500
4000
4500
5000

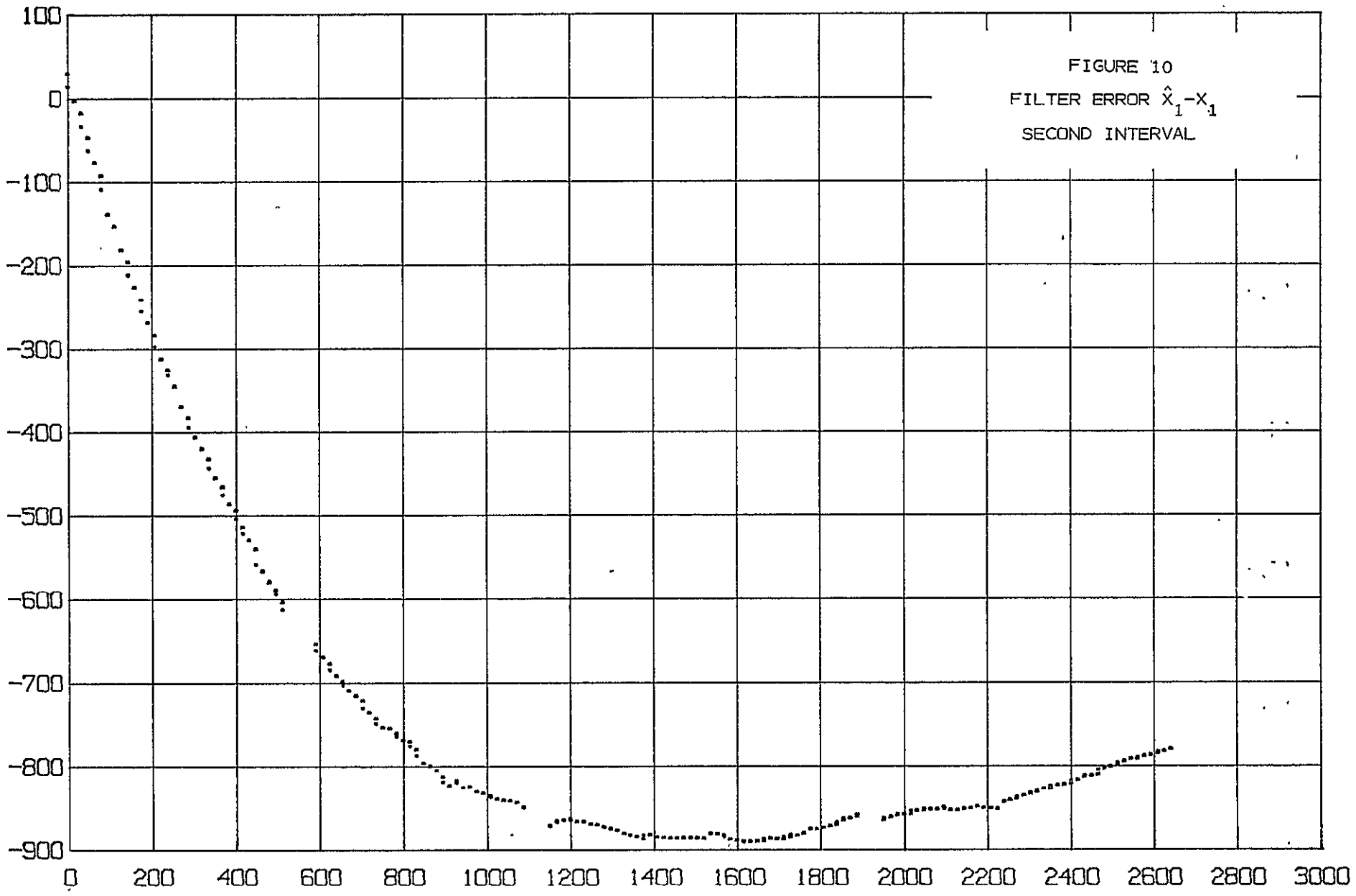
FIGURE 10
FILTER ERROR $\hat{X}_1 - X_1$
SECOND INTERVAL
100
0
-100
-200
-300
-400
-500
-600
-700
-800
-900
0
200
400
600
800
1000
1200
1400
1600
1800
2000
2200
2400
2600
2800
3000

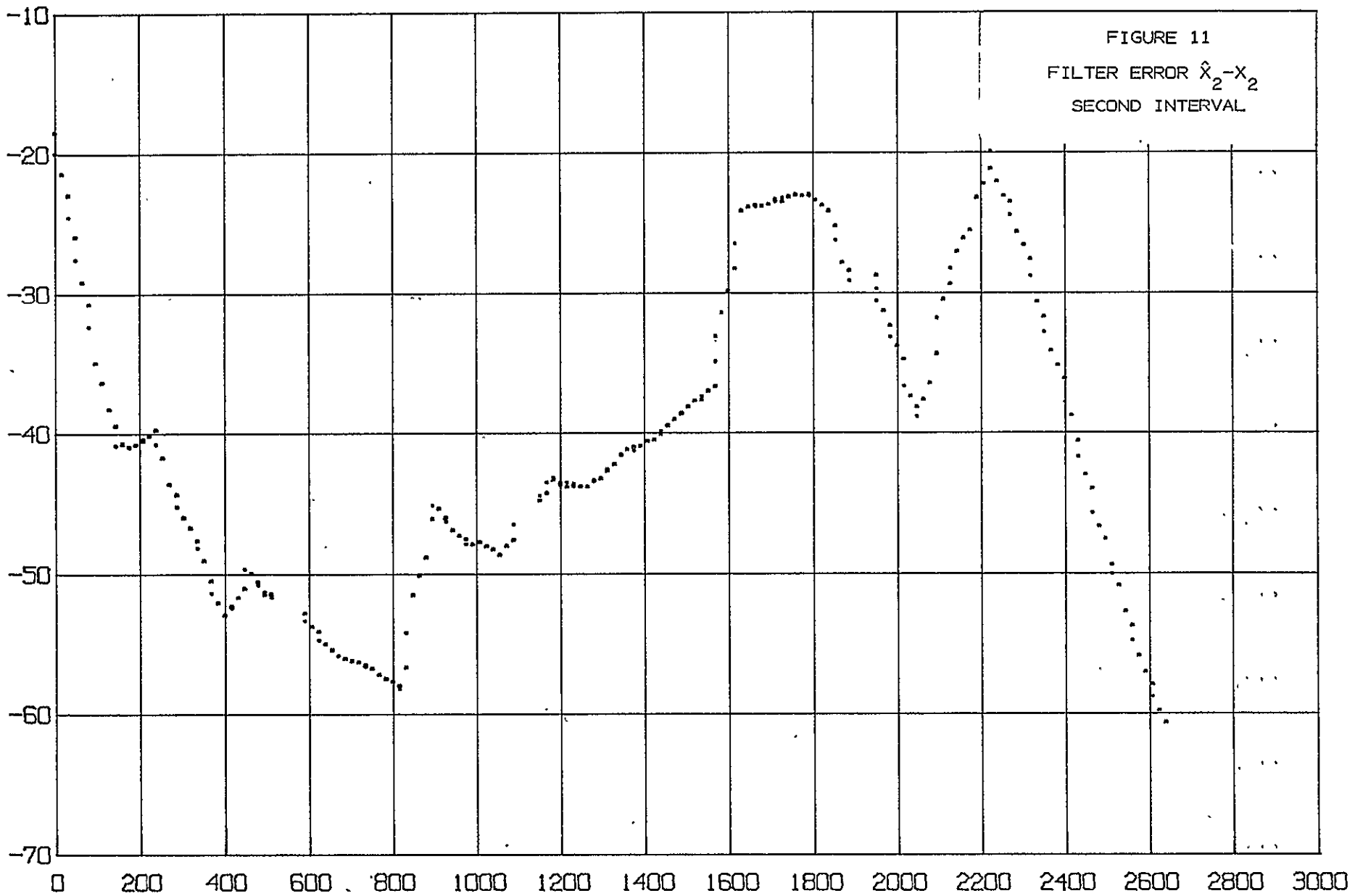
FIGURE 11
FILTER ERROR $\hat{X}_2 - X_2$
SECOND INTERVAL
-10
-20
-30
-40
-50
-60
-70
0
200
400
600
800
1000
1200
1400
1600
1800
2000
2200
2400
2600
2800
3000

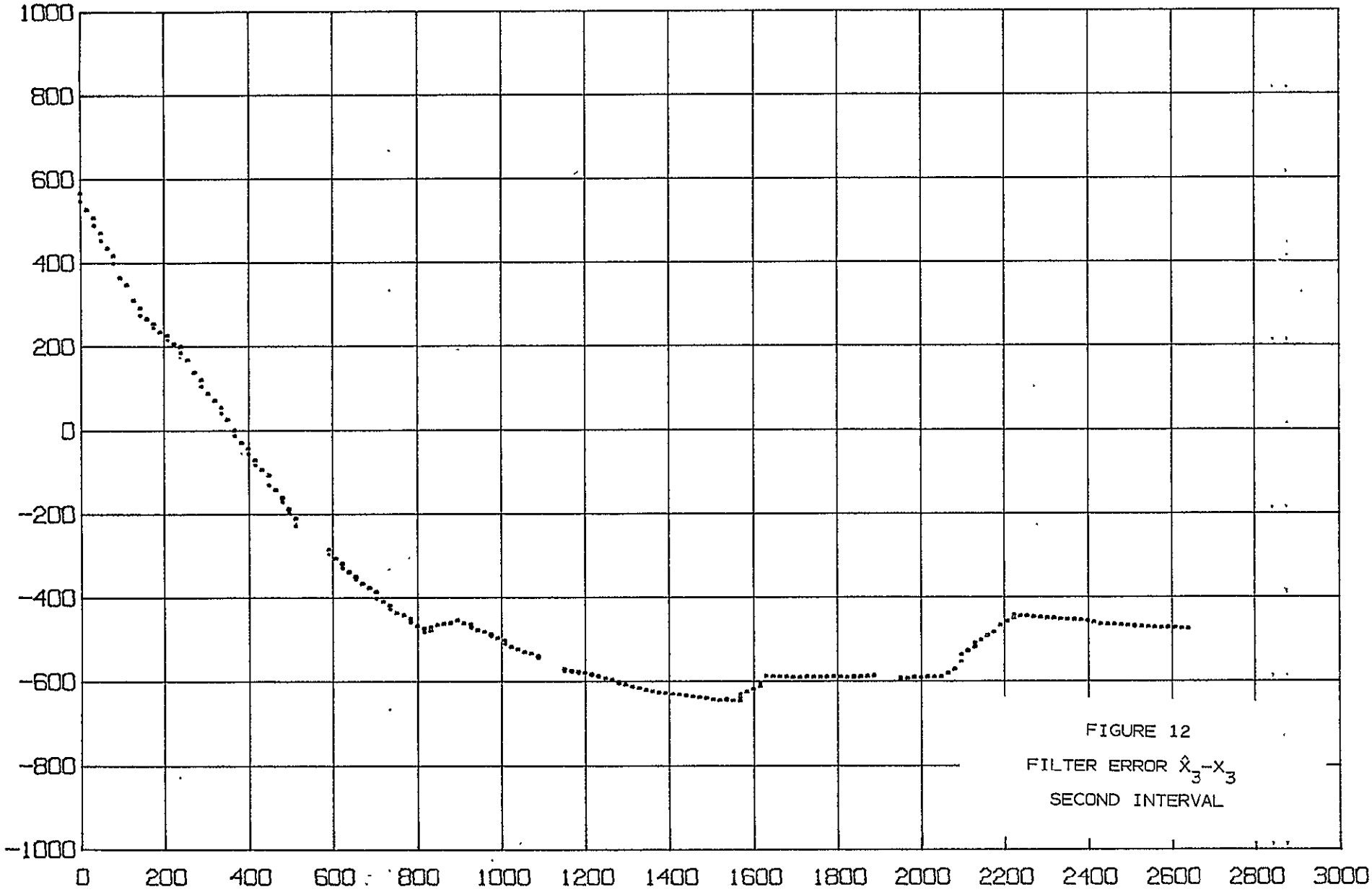

FIGURE 12

FILTER ERROR $\hat{X}_3 - X_3$

SECOND INTERVAL

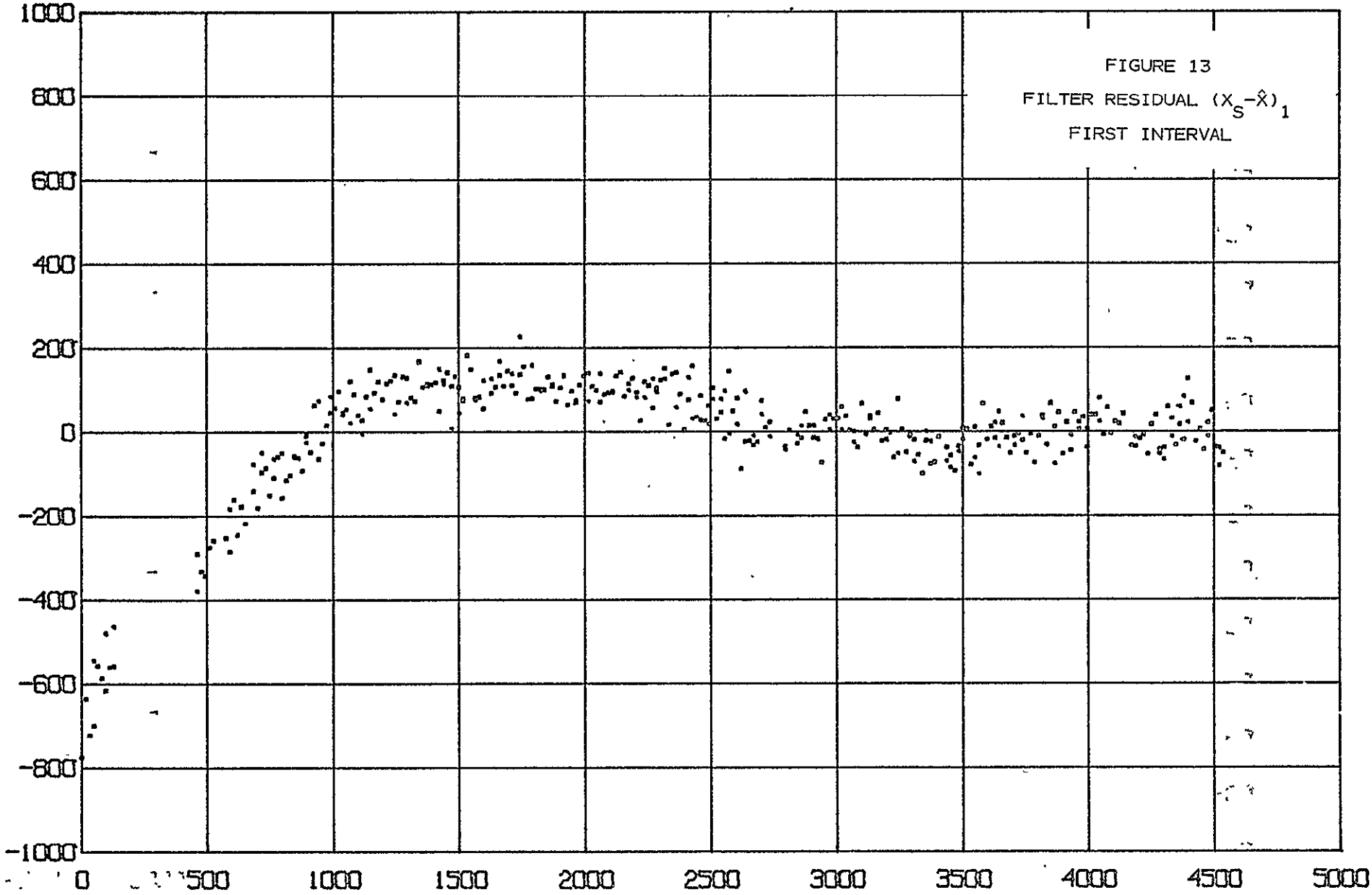
FIGURE 13
FILTER RESIDUAL $(X_S - \hat{X})_1$
FIRST INTERVAL
1000
800
600
400
200
0
-200
-400
-600
-800
-1000
0
500
1000
1500
2000
2500
3000
3500
4000
4500
5000

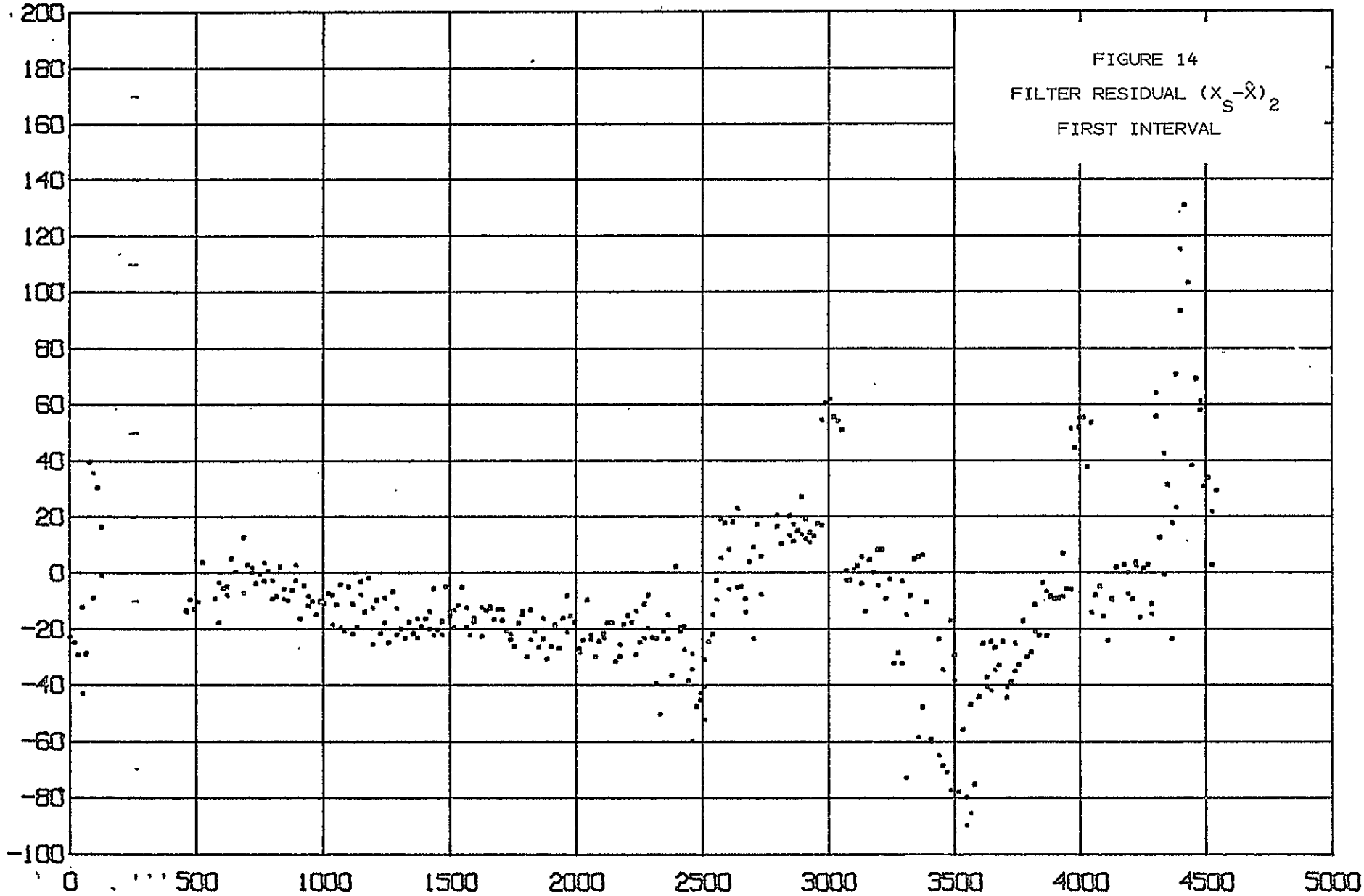
FIGURE 14
FILTER RESIDUAL $(X_S - \hat{X})_2$
FIRST INTERVAL
200
180
160
140
120
100
80
60
40
20
0
-20
-40
-60
-80
-100
0
500
1000
1500
2000
2500
3000
3500
4000
4500
5000

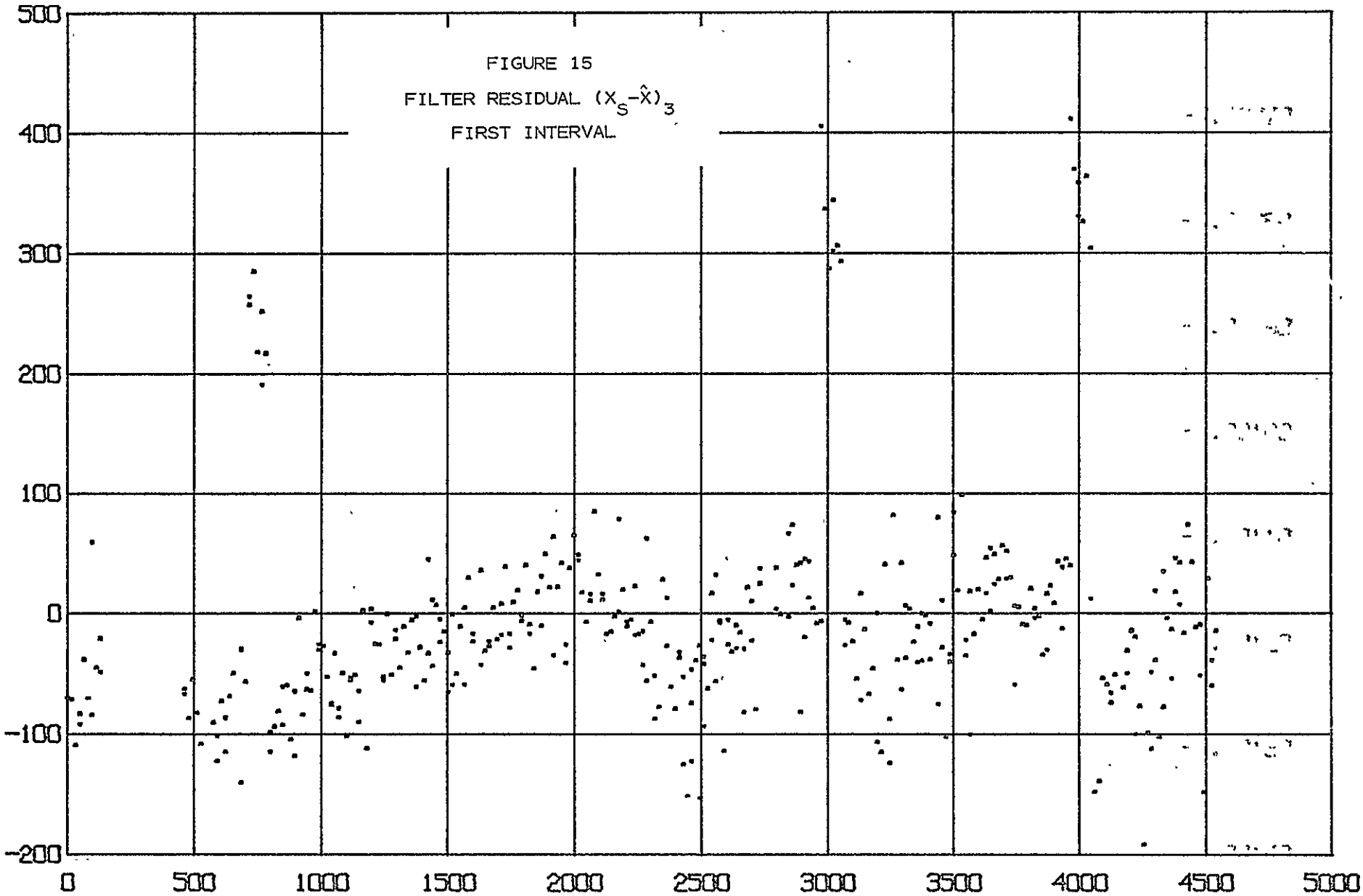
FIGURE 15
FILTER RESIDUAL $(X_S-\hat{X})_3$
FIRST INTERVAL
500
400
300
200
100
0
-100
-200
0
500
1000
1500
2000
2500
3000
3500
4000
4500
5000

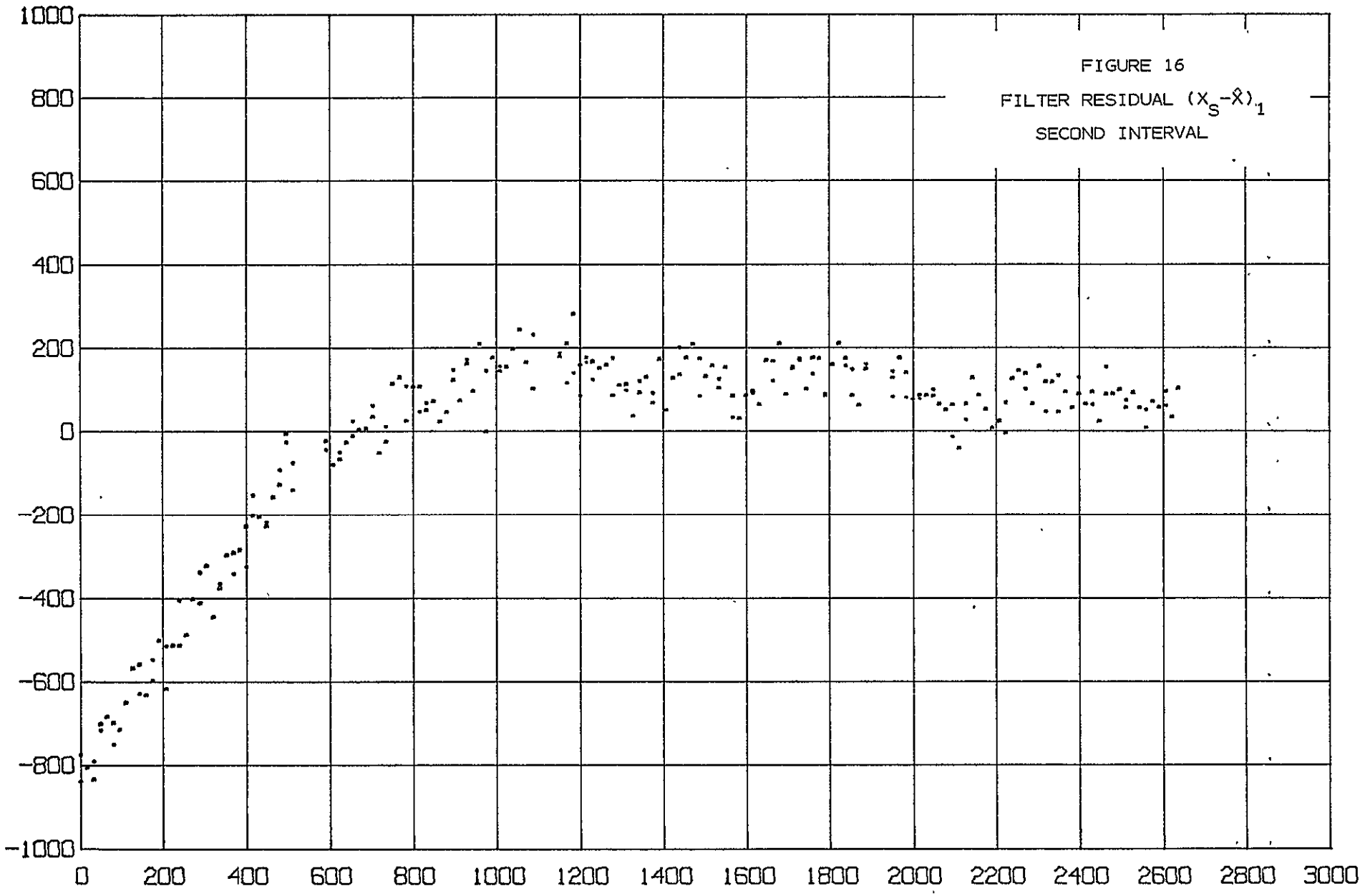

FIGURE 16

FILTER RESIDUAL $(X_S - \hat{X})_1$

SECOND INTERVAL

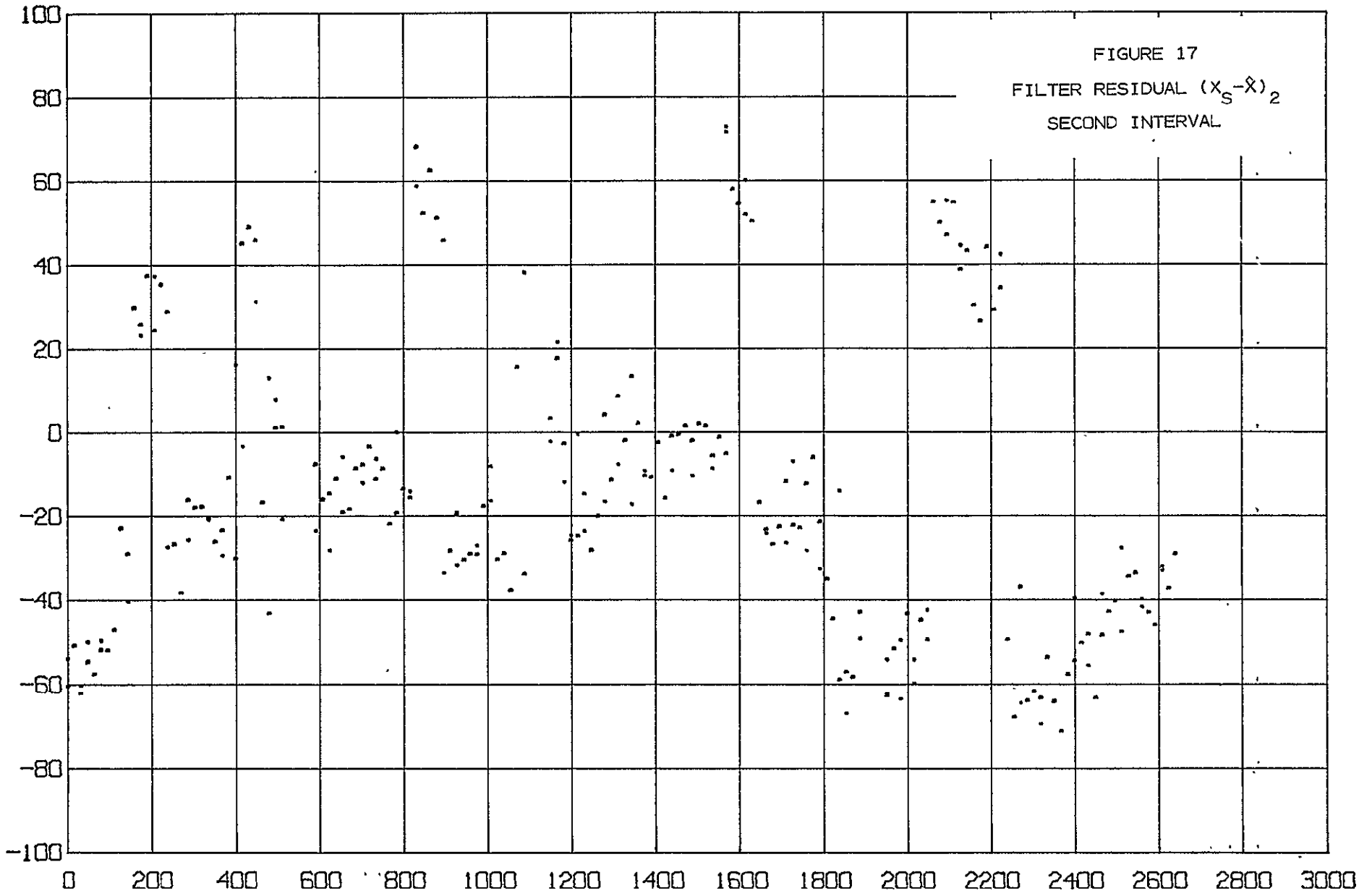
FIGURE 17
FILTER RESIDUAL $(X_S - \hat{X})_2$
SECOND INTERVAL
100
80
60
40
20
0
-20
-40
-60
-80
-100
0
200
400
600
800
1000
1200
1400
1600
1800
2000
2200
2400
2600
2800
3000

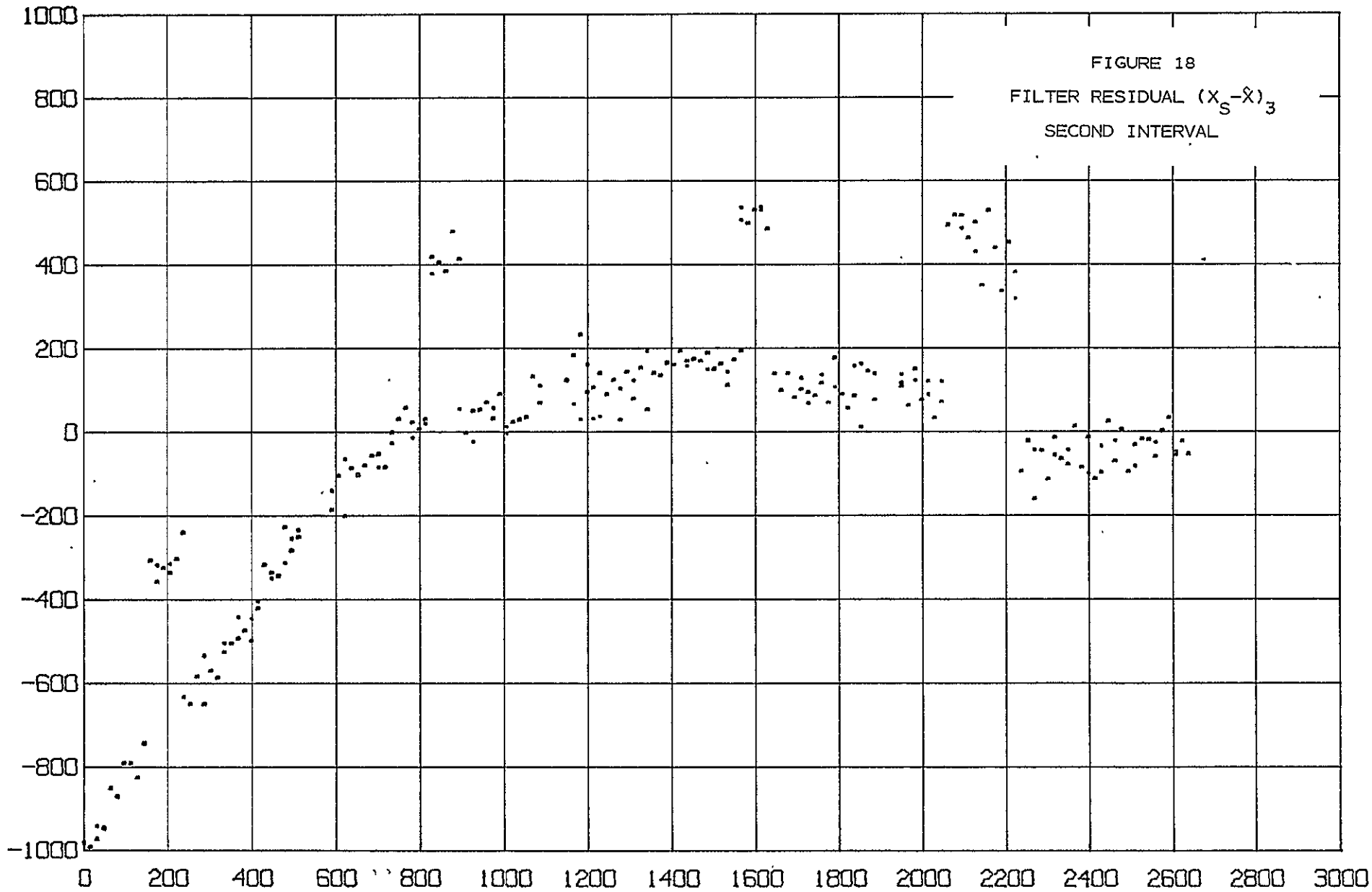
FIGURE 18
FILTER RESIDUAL $(X_S-\hat{X})_3$
SECOND INTERVAL
1000
800
600
400
200
0
-200
-400
-600
-800
-1000
0
200
400
600
800
1000
1200
1400
1600
1800
2000
2200
2400
2600
2800
3000

3.3 Euler Angle Errors

Despite the extremely large values of filter errors, the Euler angle errors were usually quite small, as the analysis (Section 2.2(3)) predicted. The largest values observed in the two runs appear in Table 1. The times at which these values occur are very highly correlated with the times at which the maximum values of $\hat{x}$ occur. However, the Euler angle excursions in roll and pitch are only about one-seventh as large as the central angle errors implied by the position errors.

Figures 19-24 show Euler angle errors (radians) for the two intervals. Notice the almost perfect correlation of $\delta\phi$ with the filter error $\hat{x}_3 - x_3$ and the correlation of $\delta\theta$ with $\hat{x}_1 - x_1$. The yaw error, $\delta\psi$, seems to correlate very well with $\hat{x}_3 - x_3$ although the geometric reasons for this are not clear.

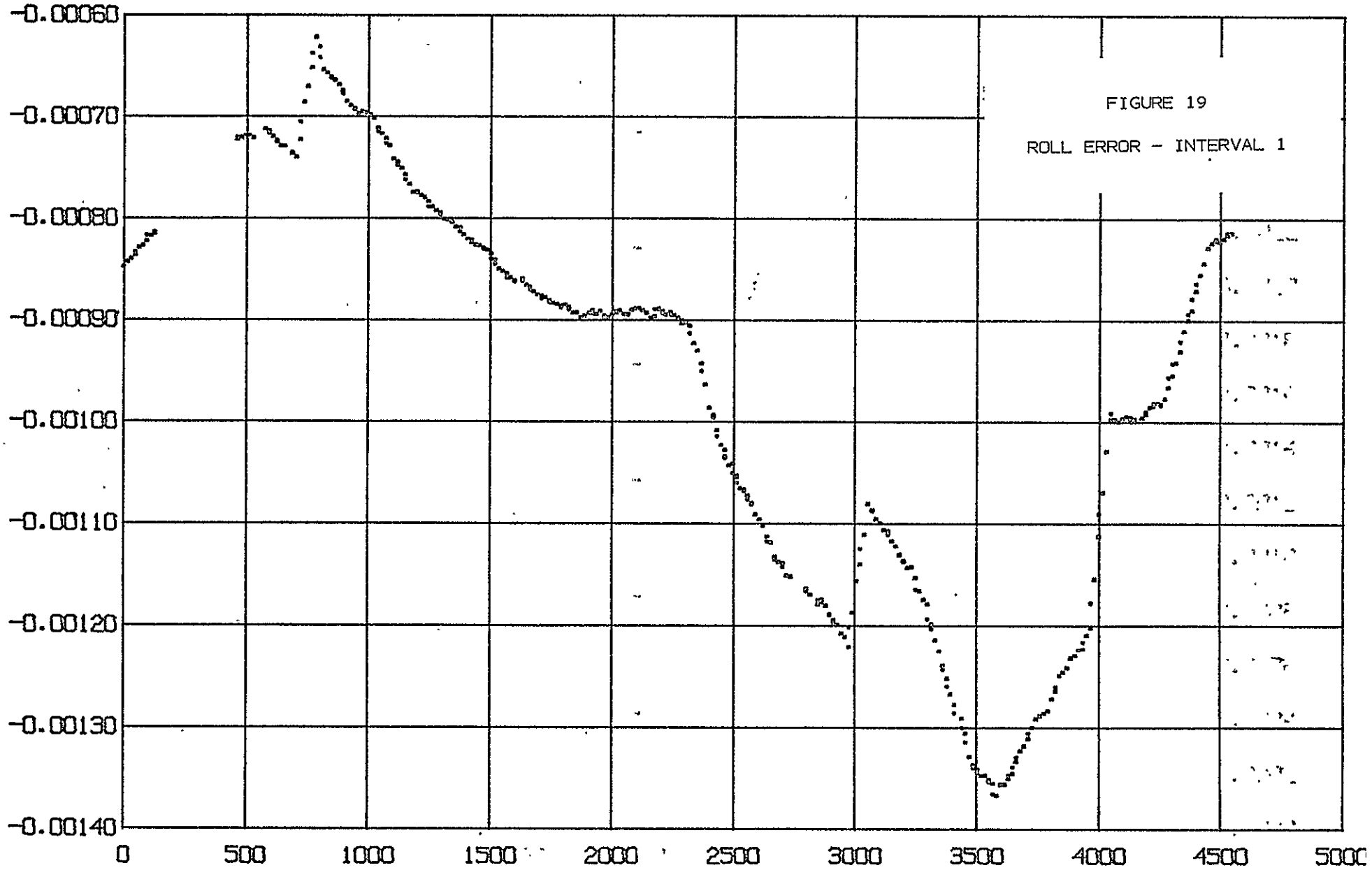

FIGURE 19

ROLL ERROR - INTERVAL 1

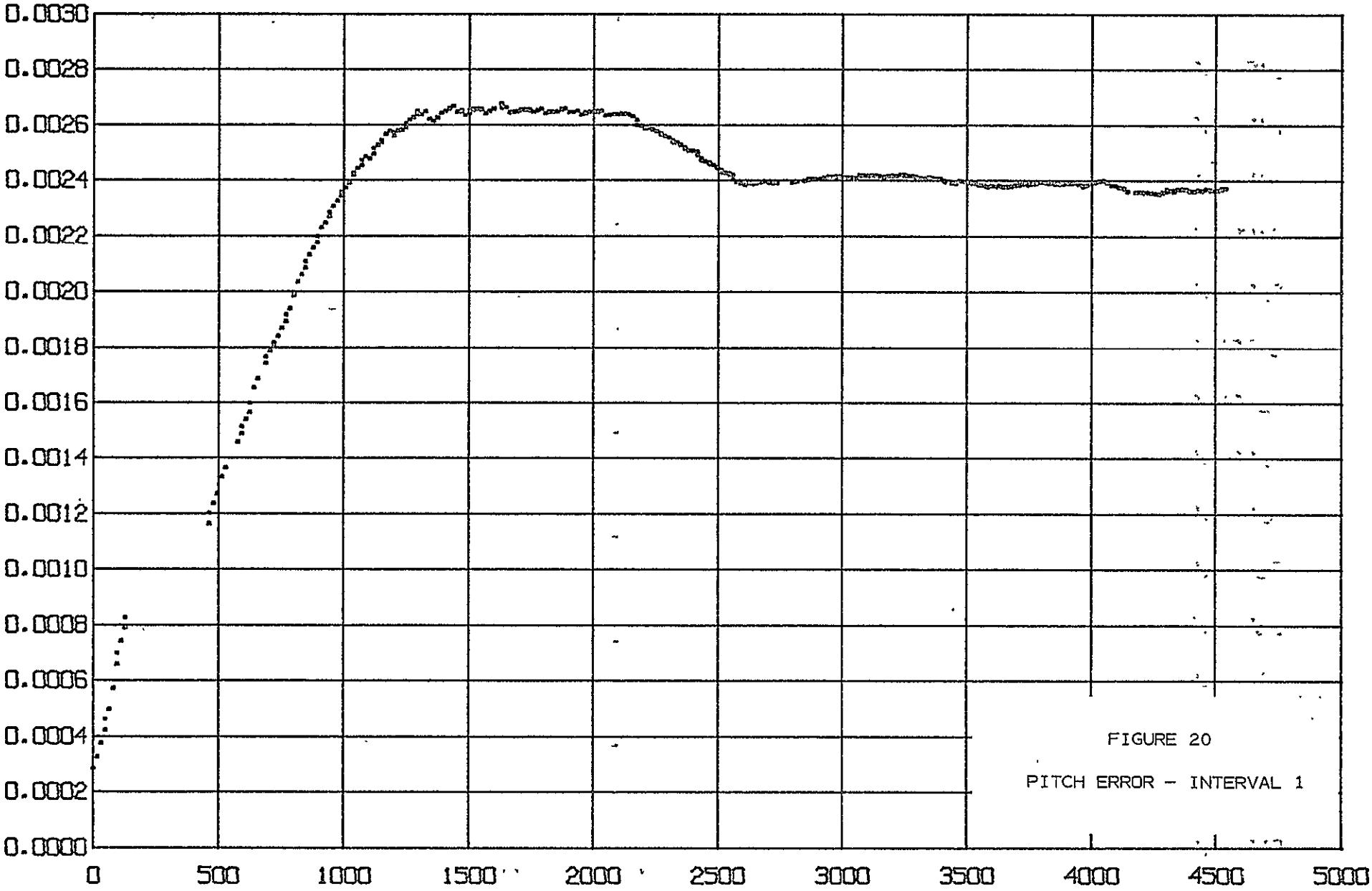

FIGURE 20

PITCH ERROR – INTERVAL 1

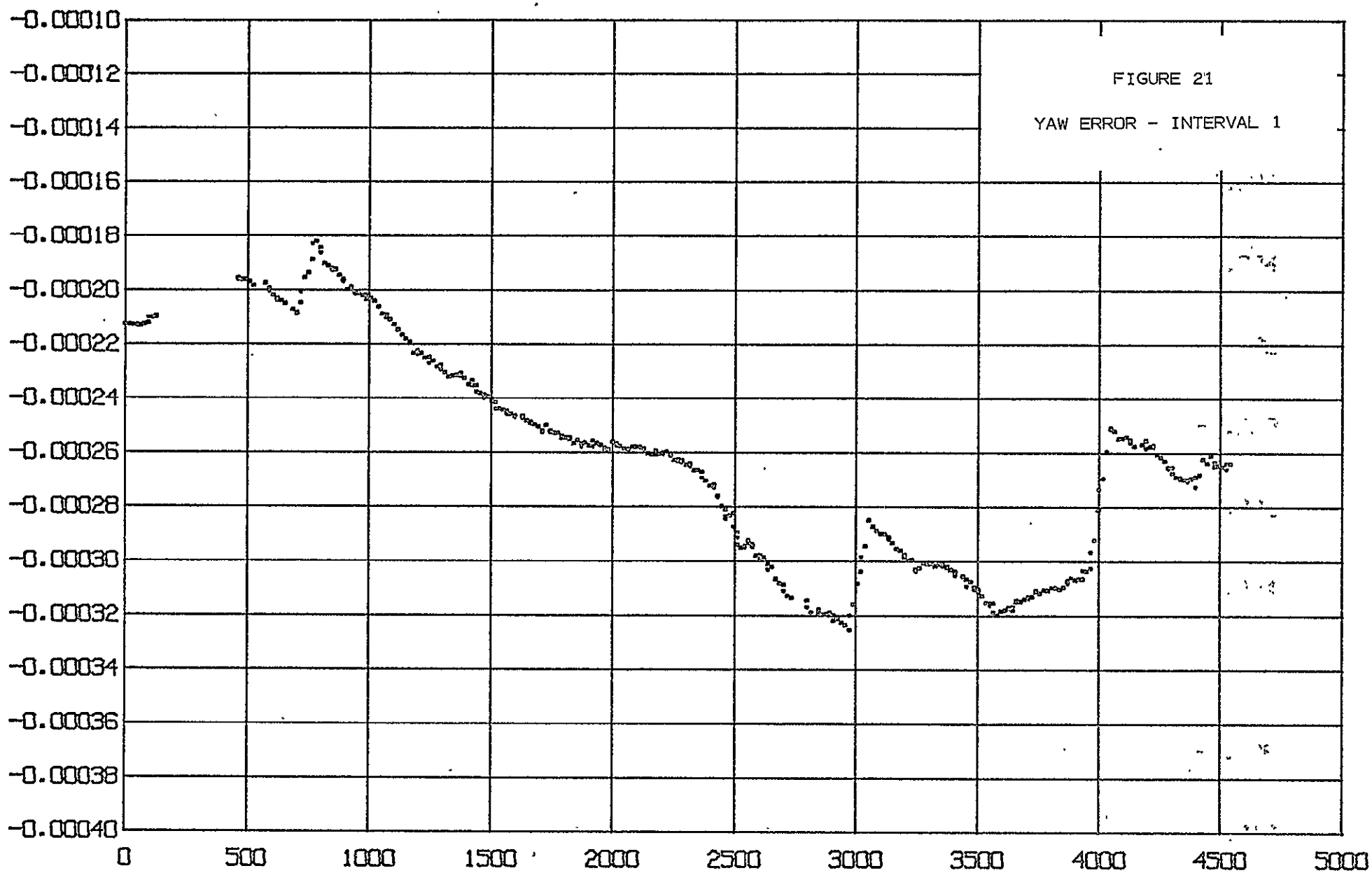
FIGURE 21
YAW ERROR - INTERVAL 1
-0.00010
-0.00012
-0.00014
-0.00016
-0.00018
-0.00020
-0.00022
-0.00024
-0.00026
-0.00028
-0.00030
-0.00032
-0.00034
-0.00036
-0.00038
-0.00040
0
500
1000
1500
2000
2500
3000
3500
4000
4500
5000

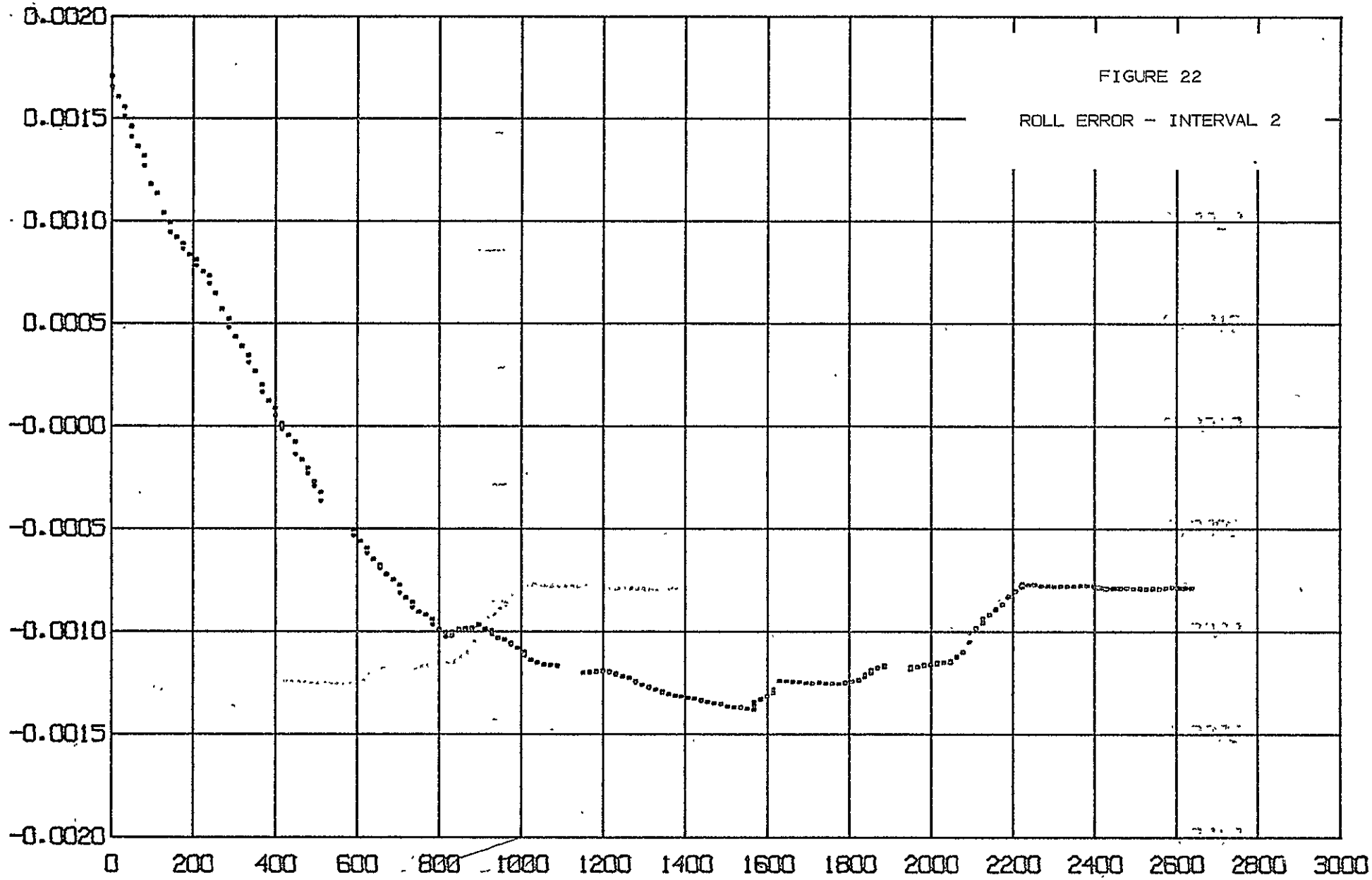
FIGURE 22
ROLL ERROR - INTERVAL 2
0.0020
0.0015
0.0010
0.0005
-0.0000
-0.0005
-0.0010
-0.0015
-0.0020
0
200
400
600
800
1000
1200
1400
1600
1800
2000
2200
2400
2600
2800
3000

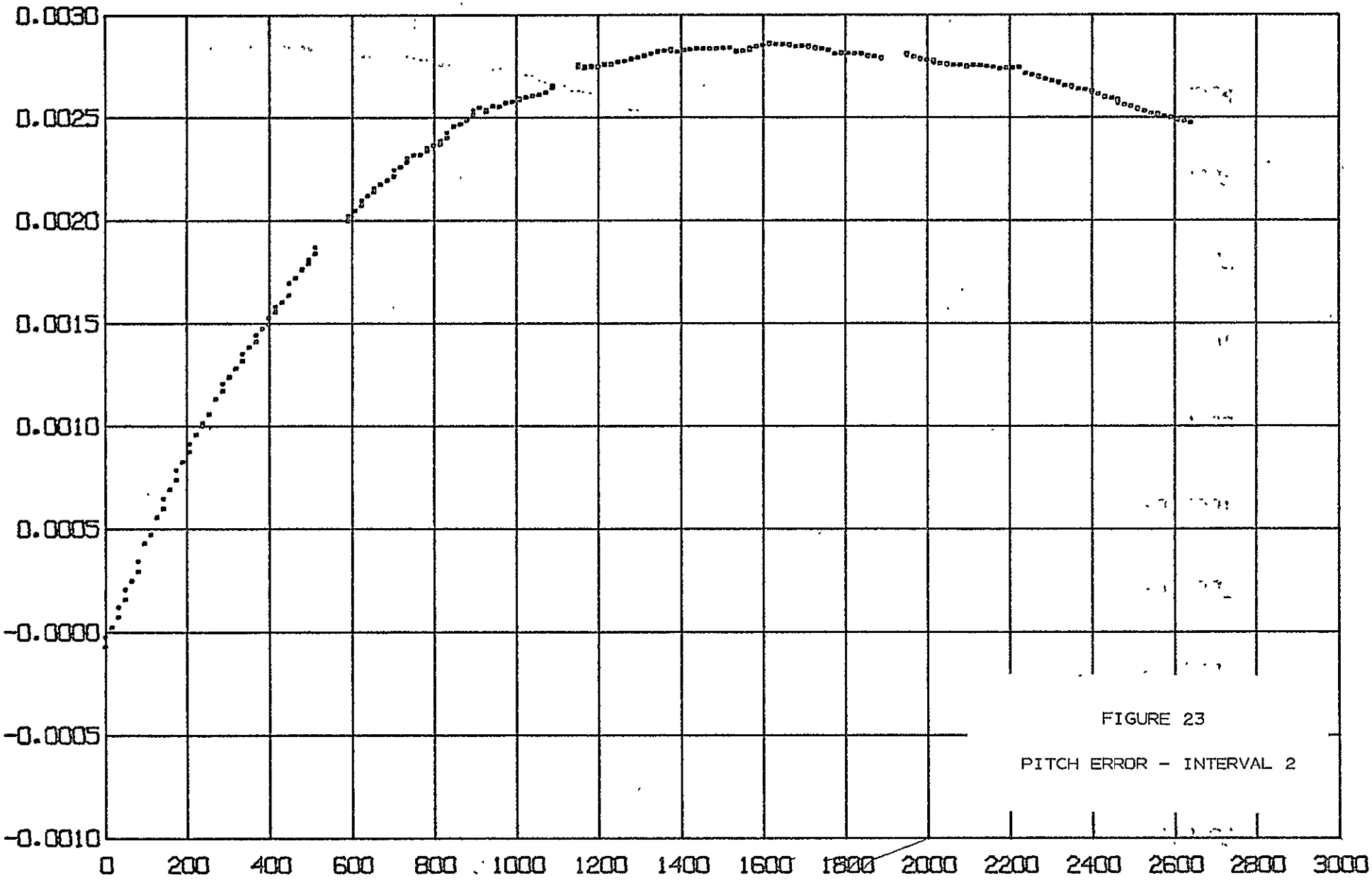

FIGURE 23

PITCH ERROR - INTERVAL 2

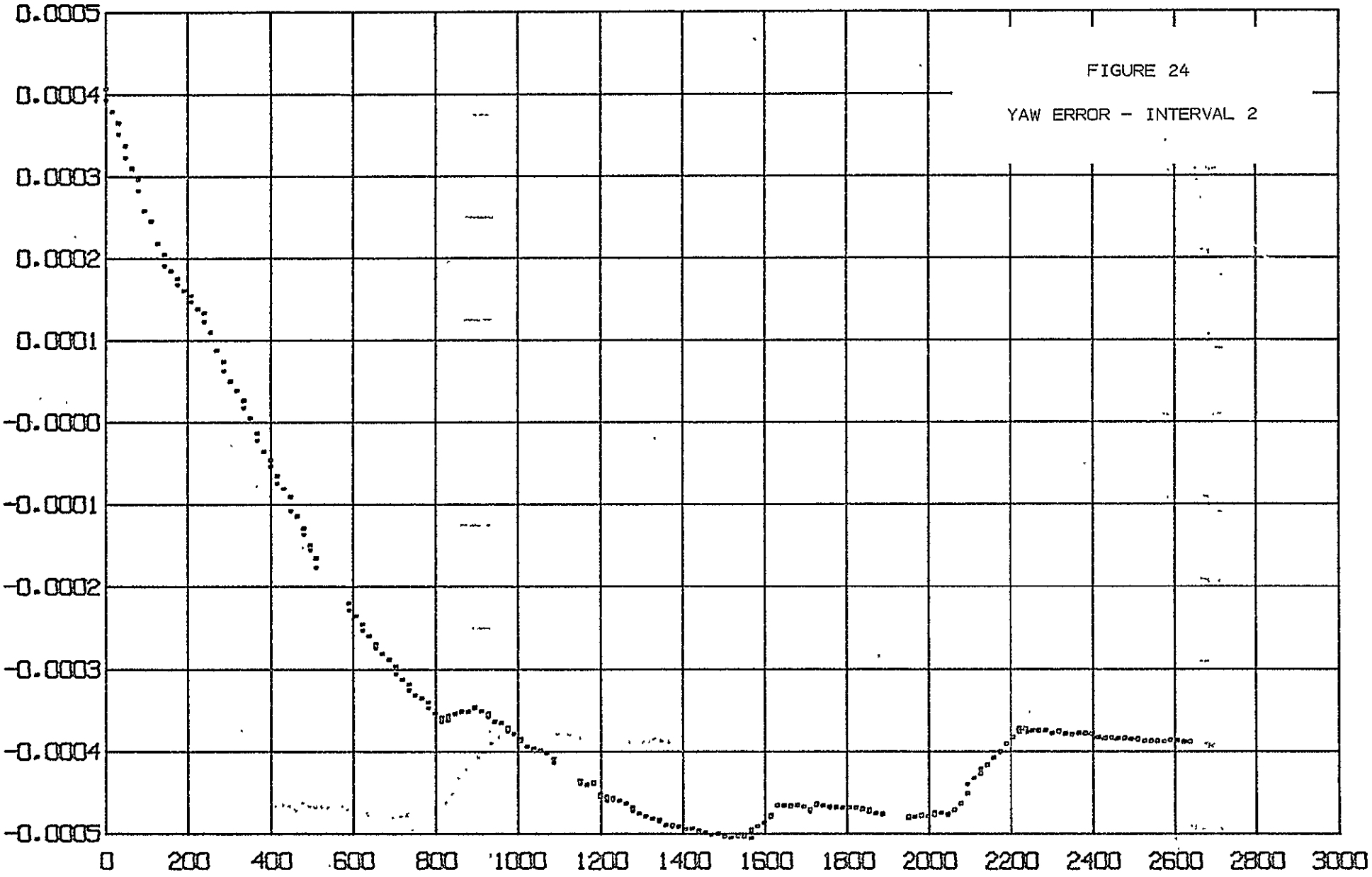
FIGURE 24
YAW ERROR - INTERVAL 2
0.0005
0.0004
0.0003
0.0002
0.0001
-0.0000
-0.0001
-0.0002
-0.0003
-0.0004
-0.0005
0
200
400
600
800
1000
1200
1400
1600
1800
2000
2200
2400
2600
2800
3000

3.4 Pierce Point Errors

In Table 2, a summary is presented of the largest pierce point errors appearing in the two data intervals. Together with the lat-long errors have been listed the contributions to pierce point errors coming from subpoint shift and from Euler angle change. Note that in longitude, the errors caused by subpoint shift and by Euler angle error tend to cancel as occured in the example (Section 2.2(3)); while in latitude, the errors added. It is not clear whether this is caused by the S/C orientation, the station - S/C geometry, or the combination of position errors. This is however a rather important point in analyzing the expected values of pierce point errors over all possible sensor errors. For instance errors in $\hat{x}_1 - x_1$ and $\hat{x}_3 - x_3$ had the same sign in both runs. Possibly the lat-long errors would change their behavior if these errors had opposite signs.

These pierce point errors represent the final touchstone of on-line orbit determination accuracy. The mean value of errors of more than 500 km in estimation of x_1 and x_3 are clearly too large; however, total absolute errors of approximately 100 km (2 counts) appear to be attainable by proper sensor calibration, and these would bring the pierce point errors down to less than 0.2° which - corresponding to an 0.03° S/C angle - is better than ATS-6 specifications.

Future applications with more stringent requirements could be met also but might require more stability and better resolution in the attitude sensors. Certainly it appears that sensor noise is a simpler problem than proper calibration and assurance that calibration parameters are either constant or have well-defined dynamics.

Figures 25-30 show pierce point errors (radians) for the two data intervals. There is an almost perfect correlation between the z component of filter error $\hat{x}_3 - x_3$, $\delta\phi$ and δ lat.

There is also very good correlation between δ long and $\delta\beta$ but neither of these show significant correlation with either the Euler angle or position errors.

FIGURE 25

LATITUDE ERROR (RAD)

FIRST INTERVAL

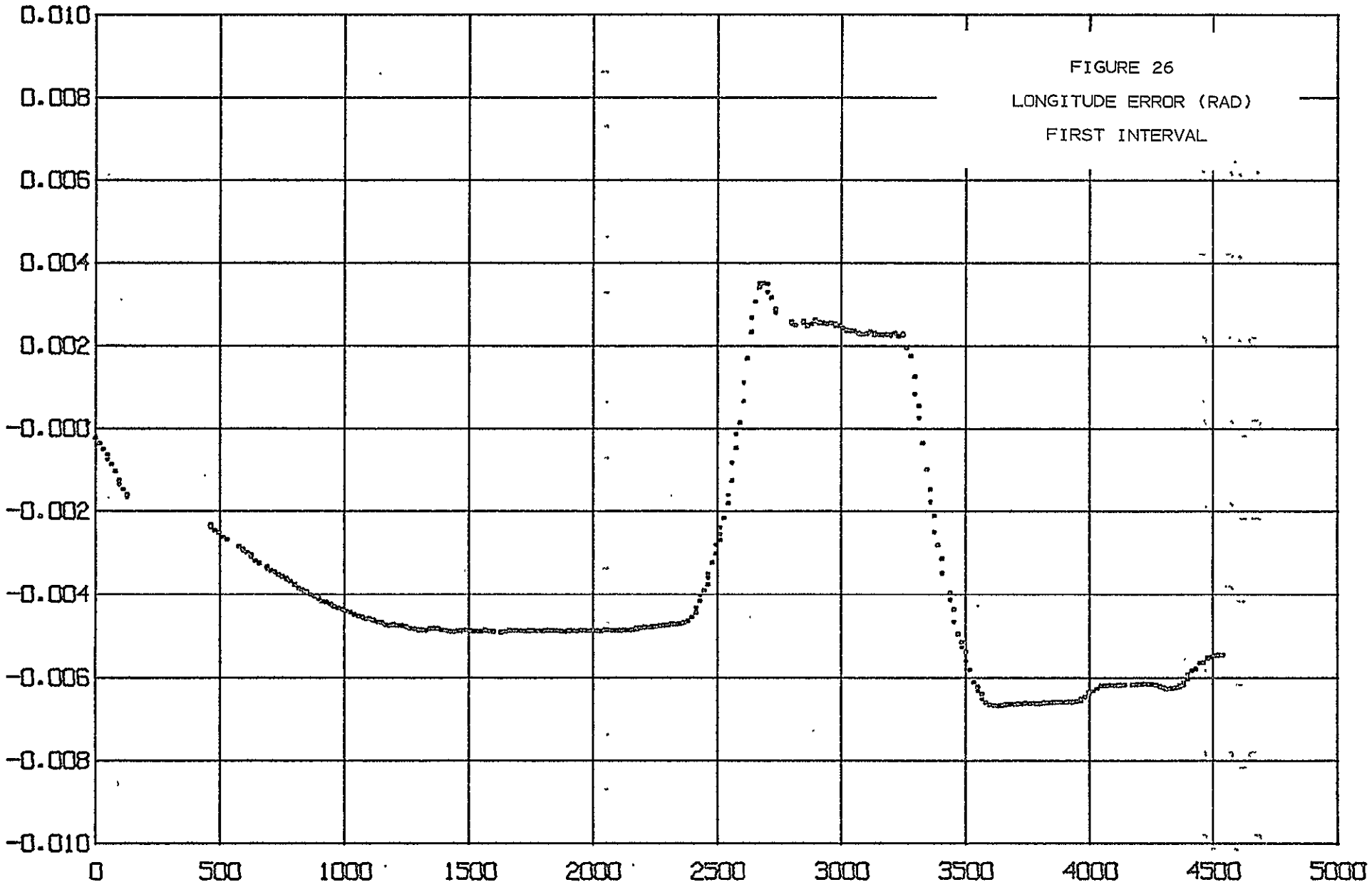
FIGURE 26
LONGITUDE ERROR (RAD)
FIRST INTERVAL
0.010
0.008
0.006
0.004
0.002
-0.000
-0.002
-0.004
-0.006
-0.008
-0.010
0
500
1000
1500
2000
2500
3000
3500
4000
4500
5000

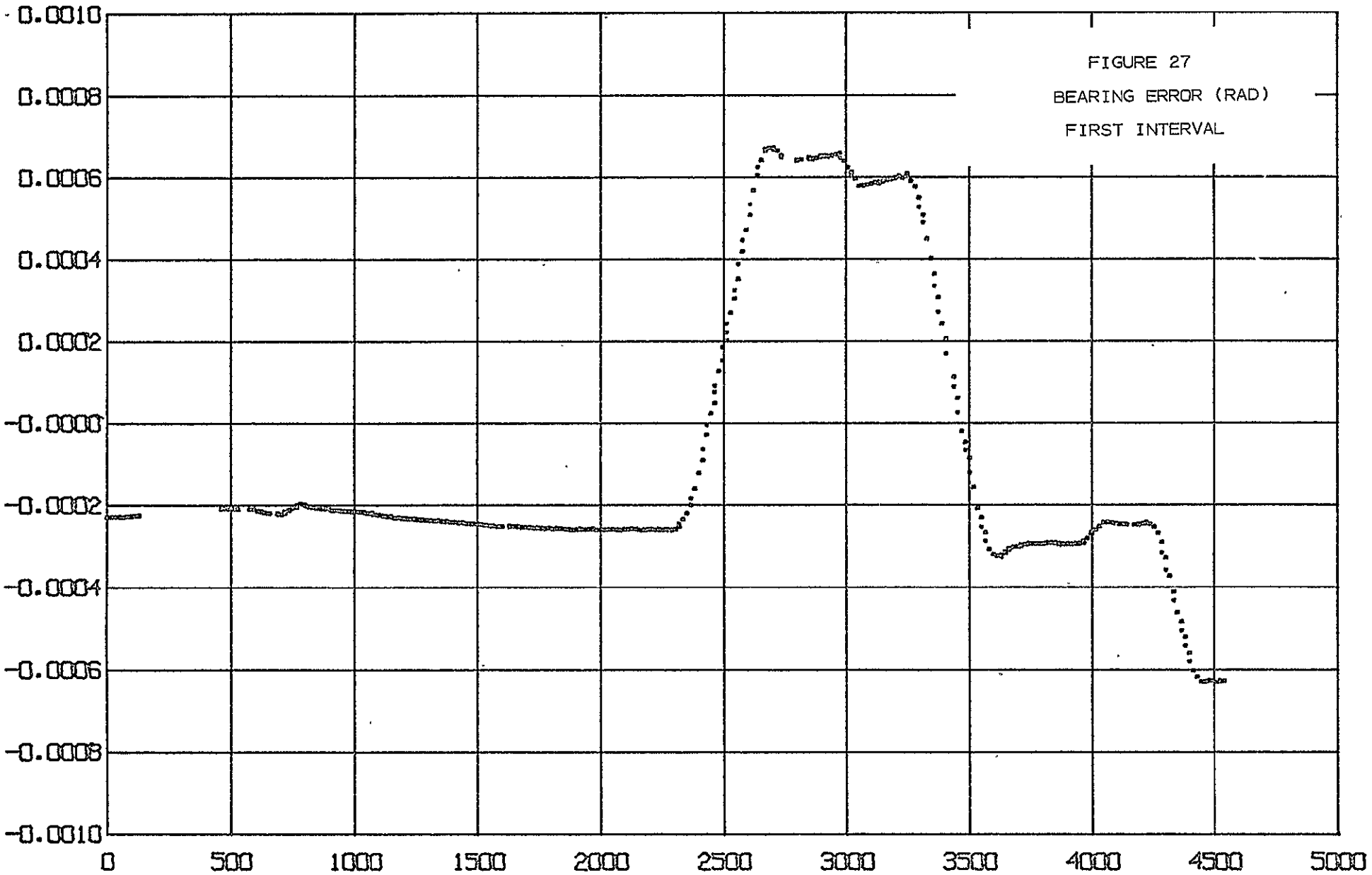
FIGURE 27
BEARING ERROR (RAD)
FIRST INTERVAL
0.0010
0.0008
0.0006
0.0004
0.0002
-0.0000
-0.0002
-0.0004
-0.0006
-0.0008
-0.0010
0
500
1000
1500
2000
2500
3000
3500
4000
4500
5000

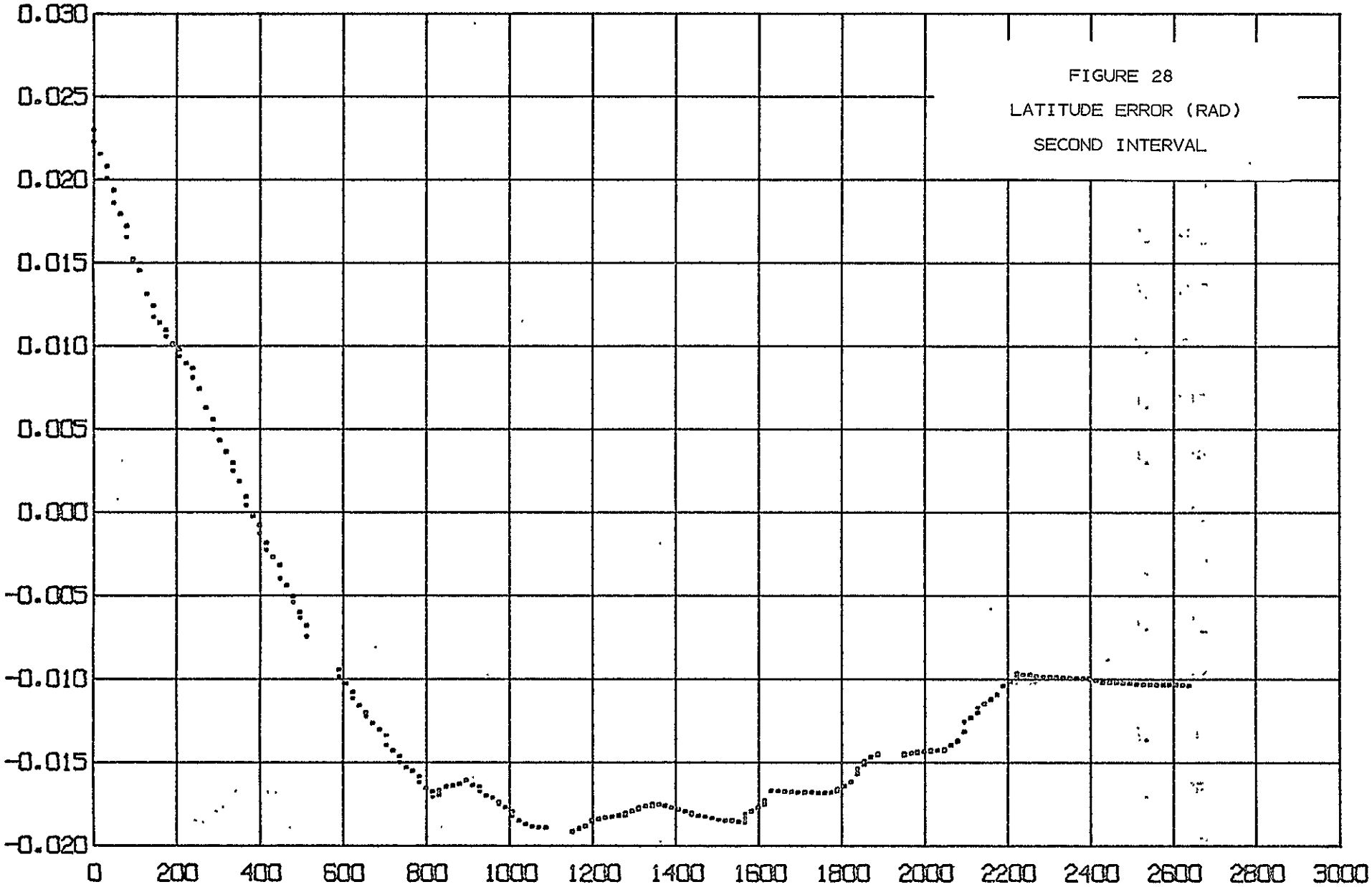
FIGURE 28
LATITUDE ERROR (RAD)
SECOND INTERVAL
0.030
0.025
0.020
0.015
0.010
0.005
0.000
-0.005
-0.010
-0.015
-0.020
0
200
400
600
800
1000
1200
1400
1600
1800
2000
2200
2400
2600
2800
3000

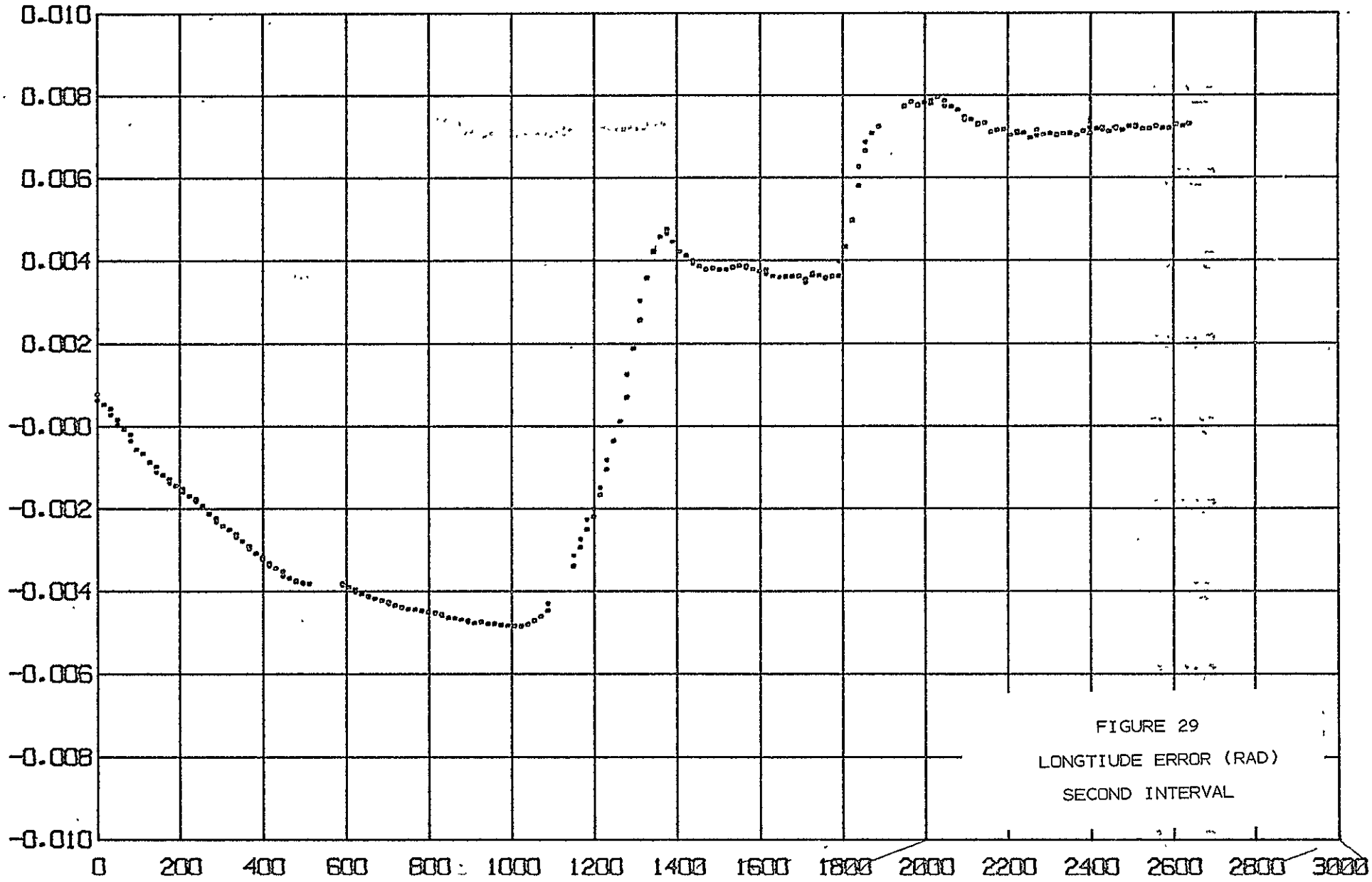

FIGURE 29

LONGTIUDE ERROR (RAD)

SECOND INTERVAL

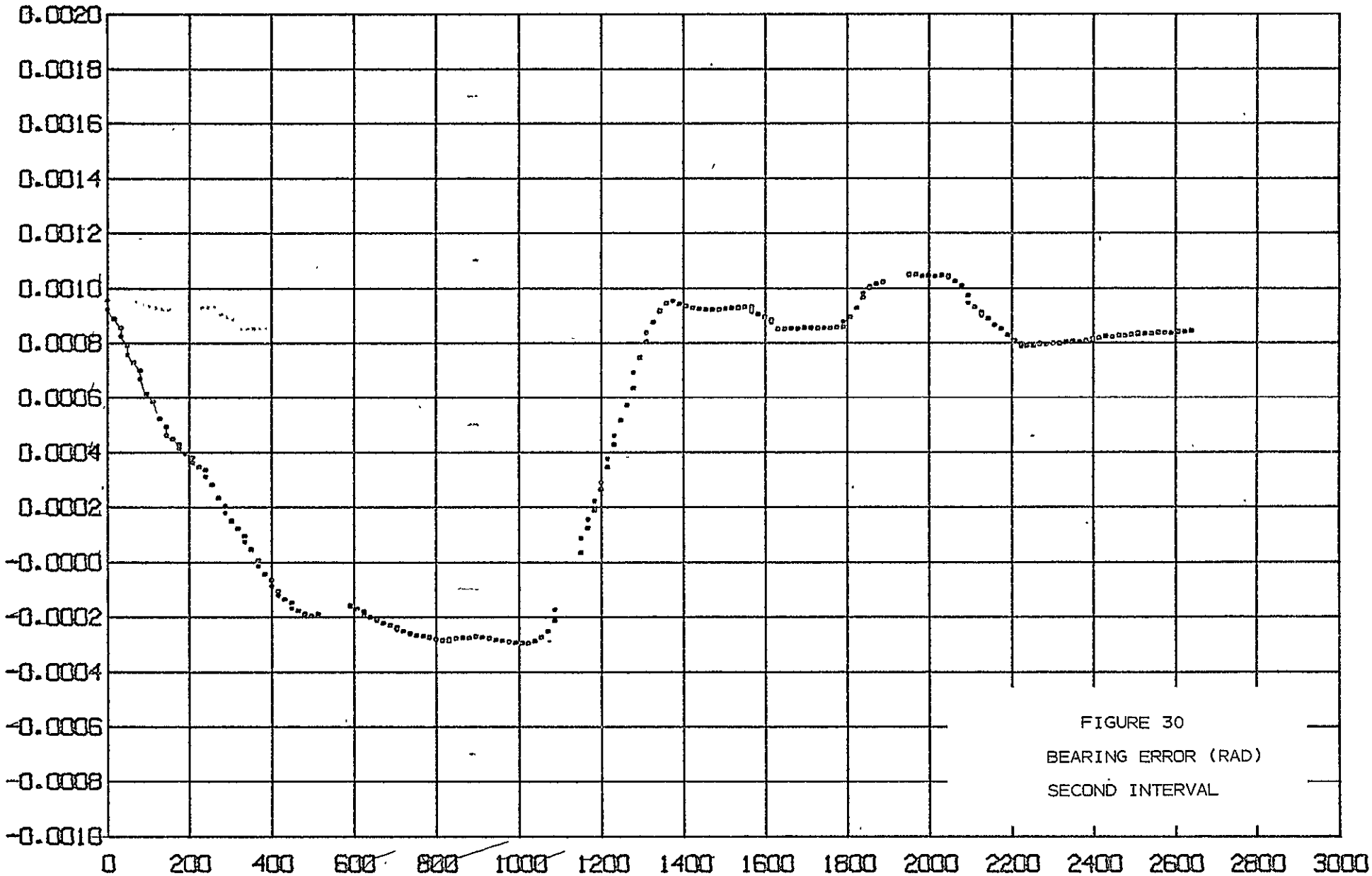

FIGURE 30

BEARING ERROR (RAD)

SECOND INTERVAL

4.0 CONCLUSIONS AND RECOMMENDATIONS

This study has demonstrated the feasibility of real-time orbit determination from attitude sensors to an accuracy of about 100 km (resulting in pierce point errors of less than 0.2°) for a S/C with three independent 2-axis sensors having error characteristics like the ESA and interferometer on ATS-6.

Experience with ATS-6 real data indicates a requirement for sensor calibration in order to achieve these results. With current calibration constants there are extremely large position biases, on the order of 900 km, leading to pierce point errors of about 1°.

Sensor error (the difference between the position pseudo-measurement and GSFC definitive orbit) has three components: A high-frequency, uncorrelated noise; a large bias, noted above; and a low frequency variation. These errors effect the estimation in distinct ways. The noise component, having a standard deviation in down-range and cross-range of about 60 km (this is consistent with sensor variations of about 1 quantum), was effectively removed by the sequential filter to a level of less than 10 km. The large biases can be easily removed by changing the ATTLMP calibration constants to a value determined by an overall, average, calibration.

The low frequency variations, having an amplitude of about 100 km, are the errors which determine the absolute error figure given above. In the current system, which neither compensates for these variations nor solves for biases, they are the factor limiting achievable accuracy.

The most important change recommended is to the ATTLMP calibration constants, forcing them to give results more consistent with the definitive orbit. This would require no structural changes.

The second change recommended is to modify the T/M reduction program so that the interferometer calibration mode is used to adjust the pertinent model parameters. This is a structural (programming) change.

The evidence of this study shows that these two changes will achieve system accuracy of about 100 km. To improve accuracy beyond this would require analysis

of data over the entire span obtained during Sensor Data Acquisition to evaluate attitude dependent effects and over an extended time period to evaluate temporal and temperature effects.

To avoid these data reduction tasks, the feasibility of accurate real-time bias identification via an extension of the existing FILTER could be investigated.

Recommended changes to FILTER in the present system are few. To guarantee all the accuracy possible in the triangulation, it would be desirable to operate in extended precision in the calculation of "sensed" position. More accurate orbit propagation models could be used, but seem to offer very little improvement in the context of 50 km errors. The system cannot be called operational until the initialization procedure is improved to remove initial transients. This problem is considered in detail in BTS-TR-75-18 describing the FILTER program.